




# Single-cell RNA sequencing identifies *eggplant* as a regulator of germ cell development in *Drosophila*

Zhipeng Sun<sup>1,2</sup> , Todd G Nystul<sup>3,\*</sup>  & Guohua Zhong<sup>1,2,\*\*</sup> 

## Abstract

*Drosophila* ovarian germline stem cells (GSCs) are a powerful model for stem cell research. In this study, we use single-cell RNA sequencing (scRNA-seq), an RNAi screen and bioinformatic analysis, to identify genes involved in germ cell differentiation, including 34 genes with upregulated expression during early germ cell development and 19 genes that may regulate germ cell differentiation. Among these, a gene we have named *eggplant* (*eggpl*) is highly expressed in GSCs and downregulated in early daughter cells. RNAi knockdown of *eggpl* causes germ cell proliferation and differentiation defects. In flies fed a rich yeast diet, the expression of *eggpl* is significantly lower and knockdown or knockout of *eggpl* phenocopies a rich diet. In addition, *eggpl* knockdown suppresses the reduction in germ cell proliferation caused by inhibition of the insulin effector PI3K. These findings suggest that downregulation of *eggpl* links nutritional status to germ cell proliferation and differentiation. Collectively, this study provides new insights into the signaling networks that regulate early germ cell development and identifies *eggpl* as a key player in this process.

**Keywords** *eggpl*; gene expression pattern; germline stem cell; GSC regulatory network; single-cell RNA sequencing

**Subject Categories** Development; Metabolism; Signal Transduction

**DOI** 10.15252/embr.202256475 | Received 14 November 2022 | Revised 27 July 2023 | Accepted 1 August 2023 | Published online 21 August 2023

**EMBO Reports (2023) 24: e56475**

## Introduction

The female reproductive system of *Drosophila melanogaster* has been well studied to understand the complex regulation of germline development (Flores *et al*, 2015; Yoshinari *et al*, 2020). Structurally, the *Drosophila* ovary comprises 16–20 ovarioles, and there are 2–3 germline stem cells (GSC) in the anterior most region of each ovariole (Hinnant *et al*, 2020). The GSCs reside in a specialized niche microenvironment and divide asymmetrically to produce one daughter cell, which maintains the stem cell identity and another daughter cell that moves away from the niche and initiates

differentiation as a cystoblast (CB). The CBs undergo four rounds of synchronous mitosis with incomplete cytokinesis to become a 16-cell cyst, with 15 nurse cells and 1 oocyte (Fig 1B). Within the stem cell niche, several short-range extrinsic signals and intrinsic stemness-promoting factors are crucial to maintain GSC self-renewal and differentiation. The action of these signals is patterned by the somatic niche cells, which comprises terminal filament cells (TFs), cap cells (CpCs) and escort cells (ECs) (Dansereau & Lasko, 2008; Wang & Cai, 2008; Liu *et al*, 2010; König *et al*, 2011; Lu *et al*, 2015; Ameku & Niwa, 2016; Banisch *et al*, 2017; Upadhyay *et al*, 2018; Tu *et al*, 2021). *Decapentaplegic* (*dpp*) is one of the necessary and sufficient niche-derived factors for GSC maintenance. A high level of *dpp* signaling activity activates the bone morphogenic proteins (BMP) signaling pathway to transcriptionally silence the expression of a differentiation promoting factor, *bag-of-marbles* (*bam*), and sustain GSC identity. In contrast, CBs positioned outside the niche experience a weaker *Dpp* signal and trigger *bam* expression for differentiation (Drummond-Barbosa, 2019). The GSCs and their progeny also signal back to ECs through the EGFR pathway to promote the encapsulation of germ cells by the ECs (Schulz *et al*, 2002). In addition, both nuclear organization and chromatin modification also play a key role in the regulation of GSC homeostasis. For example, it is reported that a linker histone H1 is intrinsically required for GSC maintenance, since the depletion of H1 in the germ cells leads to premature expression of *Bam* and GSC loss (Sun *et al*, 2015). Similarly, *scrawny* (*scny*), an H2B ubiquitin protease, is highly expressed in GSCs and suppresses methylation at lysine residues to functionally repress target genes. Loss of *scny* results in premature expression of *Bam* (Buszczak *et al*, 2009). It has also been shown that *eggless* (*egg*), a histone methyltransferase, is required for maintenance of GSC fate. Depletion of *egg* in GSC impairs self-renewal ability, while the *egg*-deficient GSCs could differentiate normally (Wang *et al*, 2011). In addition, *stonewall* (*Stwl*), a chromatin-associated protein which acts as a dominant suppressor of variegation, is enriched in GSCs (Maines *et al*, 2007). *Mei-P26* suppresses genes that are important for CB differentiation through miRNA pathway (Li *et al*, 2013). However, *zpg* is essential to initiate the differentiation in GSCs and early germ cells (Tazuke *et al*, 2002). Therefore, the proper balance of intrinsic and extrinsic gene expression is imperative for GSC self-renewal and differentiation.

1 Key Laboratory of Crop Integrated Pest Management in South China, Ministry of Agriculture and Rural Affairs, South China Agricultural University, Guangzhou, China

2 Key Laboratory of Natural Pesticide and Chemical Biology, Ministry of Education, South China Agricultural University, Guangzhou, China

3 Department of Anatomy, UCSF, San Francisco, CA, USA

\*Corresponding author. Tel: +1 415 970 6967; E-mail: todd.nystul@ucsf.edu

\*\*Corresponding author. Tel: +86 20 85280308; E-mail: guohuazhong@scau.edu.cn

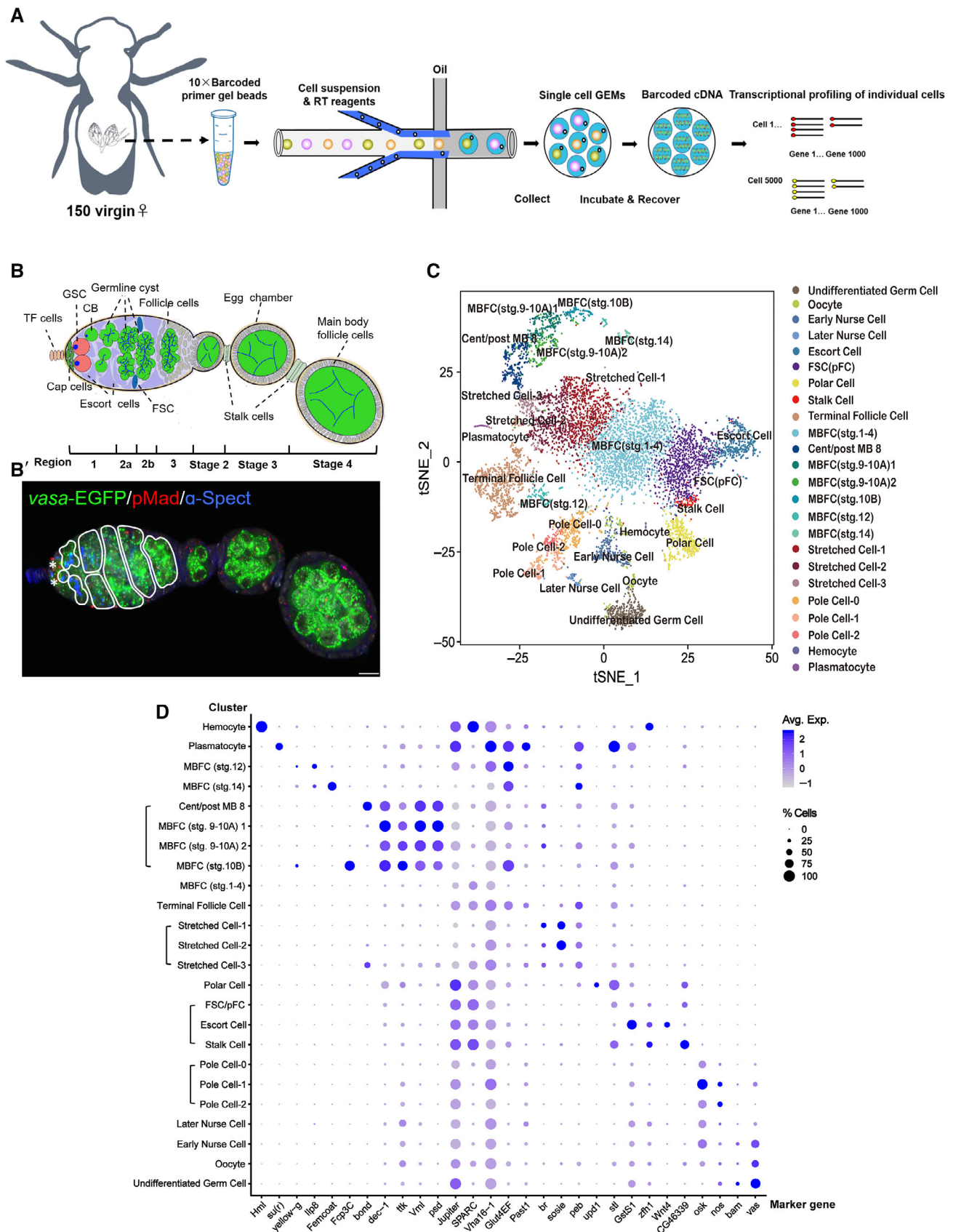


Figure 1.

**Figure 1. 10× Genomics single-cell RNA sequencing on adult *Drosophila* ovary.**

- A Schematic of experimental workflow for cell capture and single-cell data analysis.
- B Illustration of a *Drosophila* ovariole, describing asymmetric divisions of GSCs and CBs, which divide four times to produce developing germline cysts. By region 2b, the 16-cell cyst is completely formed and surrounded by follicle cells. As the cyst moves down to Region 3, the egg chamber containing 1 oocyte and 15 nurse cells is formed and ready to bud off.
- B' The *vasa-EGFP* line was used to visualize all germ cells along germline. Anti-pMad (red) was used to label GSCs (asterisk), while anti- $\alpha$ -Spectrin (blue) was used to stain spectrosomes (round dot) and branched fusomes. The scale bar is 10  $\mu$ m.
- C A t-SNE plot of 24 distinct cell clusters marked with different colors.
- D A dot plot of scaled expression of selected typical marker genes in each cell type.

Source data are available online for this figure.

An additional layer of regulation of the GSC niche comes from signals that communicate with the availability of a rich diet. On high protein diet, GSCs and their descendants exhibit an increased rate of division and differentiation, and this response to diet is regulated by evolutionarily conserved insulin signaling pathway. Neurosecretory cells in the brain produce the insulin-like peptides (DILPs), which directly regulate the G2 phase of GSC division and stimulate cyst growth (LaFever & Drummond-Barbosa, 2005; Hsu et al, 2008). In flies fed a yeast-rich diet, the ovary size and egg production are significantly increased (Drummond-Barbosa & Spradling, 2001). This is due to the action of insulin on the GSC niche cells, which facilitates GSC proliferation and maintenance, in part by promoting the extension of EC membranes to wrap around GSCs and cysts (Su et al, 2018). The membrane extensions are regulated by a membrane protein, Failed axon connections (Fax), which is induced by S6K activation downstream of the insulin receptor. Insulin also acts on cap cells to promote Notch signaling and stimulate the physical adhesion between cap cells and GSCs through E-cadherin (Hsu & Drummond-Barbosa, 2009). However, the downstream response in germ cells to these nutrient-activated cues is not well understood.

In this study, we identified 34 genes that are differentially expressed during early germ cell development and found that 19 of these are required for germ cell function. These genes were identified by scRNA-seq analysis of adult wildtype ovaries and validated by assessing expression patterns *in vivo* and performing an RNAi screen for an increase or decrease in GSC number, GSC loss, and tumor formation. In addition, network analysis of the differentially expressed genes in undifferentiated germ cell-1 and -2 clusters revealed several common nodes. Among the genes, we identified an uncharacterized gene, *CG32814*, which we renamed *eggplant* (*eggpl*). We found that *eggpl* was specifically expressed in GSCs at the transcriptional level, but *Eggpl* protein was detectable in germ cells throughout Region 1. We found that *eggpl* was also expressed in larval male and female gonads and in adult testes as well. We also found an increase in the number of both BrdU<sup>+</sup> and PH3<sup>+</sup> cysts, and that the ovaries were larger in flies in which *eggpl* was depleted, either by RNAi or in a CRISPR knockout. Similarly, in flies fed a rich yeast diet, *eggpl* expression was reduced and *eggpl* knockdown or knockout suppressed the decrease in germ cell proliferation caused by inhibition of PI3K. Taken together, these findings reveal genes that control early germ cell differentiation and coordinate the rate of germline stem cell division with nutrient availability.

## Results

### Overview of a single-cell RNA transcriptional atlas of the *Drosophila* ovary

To characterize the transcriptional profile of ovarian cell types, we performed scRNA-seq on 7-day-old adult *Drosophila* ovaries by using the 10× Genomics Chromium system to complete the complementary DNA (cDNA) synthesis and amplification, library preparation, and sequencing process (Fig 1A). We then used t-Stochastic-Neighbor Embedding (t-SNE) in Seurat (Satija et al, 2015) to reduce the dimensionality and visualize the unsupervised cell distribution. Twelve cell clusters (Fig EV1A and A') were first classified based on their unique transcriptional profiles with the default resolution.

We further assigned cell types using canonical marker genes and adjusted the Seurat resolution as needed, resulting in 24 distinct clusters in total (Fig 1C and D). The two clusters (cluster 6 and cluster 8) that expressed germ cell marker *vasa* (Lasko & Ashburner, 1988) were combined into one germ cell cluster (Fig EV1A'). We then divided the combined cluster into four sub-clusters (undifferentiated germ cell, oocyte, early nurse cell, and later nurse cells) based on distinctions between the transcriptional profiles revealed by unsupervised clustering and identification of stage-specific markers (Figs 2A and EV1D). Both *nanos* which is maternally loaded into the pole plasm and translated after fertilization (Deshpande et al, 1999) and *osk* which is highly enriched in germ plasm and accumulated in pole cells (Kim-Ha et al, 1991; Eichler et al, 2020) were used to identify three subtypes of pole cell clusters at a resolution value of 0.5 ( $R = 0.5$ ). The stalk cell cluster was enriched in the expression of *zfh-1* (Tatapudy et al, 2021), *stl* and *CG46339*, as expected (Rust et al, 2020a). The EC cluster was identified by the enrichment for cells expressing *Wnt4* and *GstS1* (Rust et al, 2020a), and the polar cell cluster was identified by a known marker *upd1* (Silver & Montell, 2001) at default resolution value ( $R = 1$ ). Three subpopulations of stretch cells were distinguished by several marker genes, including *peb* (Sun & Deng, 2005), *sosie* (Urwyler et al, 2012), *br* (Tzolovsky et al, 1999), *past1*, *Glut4EF*, and *Vha16-1* (Jevitt et al, 2020a) at 0.5 resolution value ( $R = 0.5$ ), and the terminal follicle cell cluster was identified by the expression of *past1*. The expression of *SPARC* and *Jupiter* was used to identify the cluster containing main body follicle cells from Stage 1–4 follicles (1–4 MBFC; Rust et al, 2020a). Four subclusters such as MBFC (stg. 9–10A) 1, MBFC (stg. 9–10A) 2, MBFC (stg. 10B), and

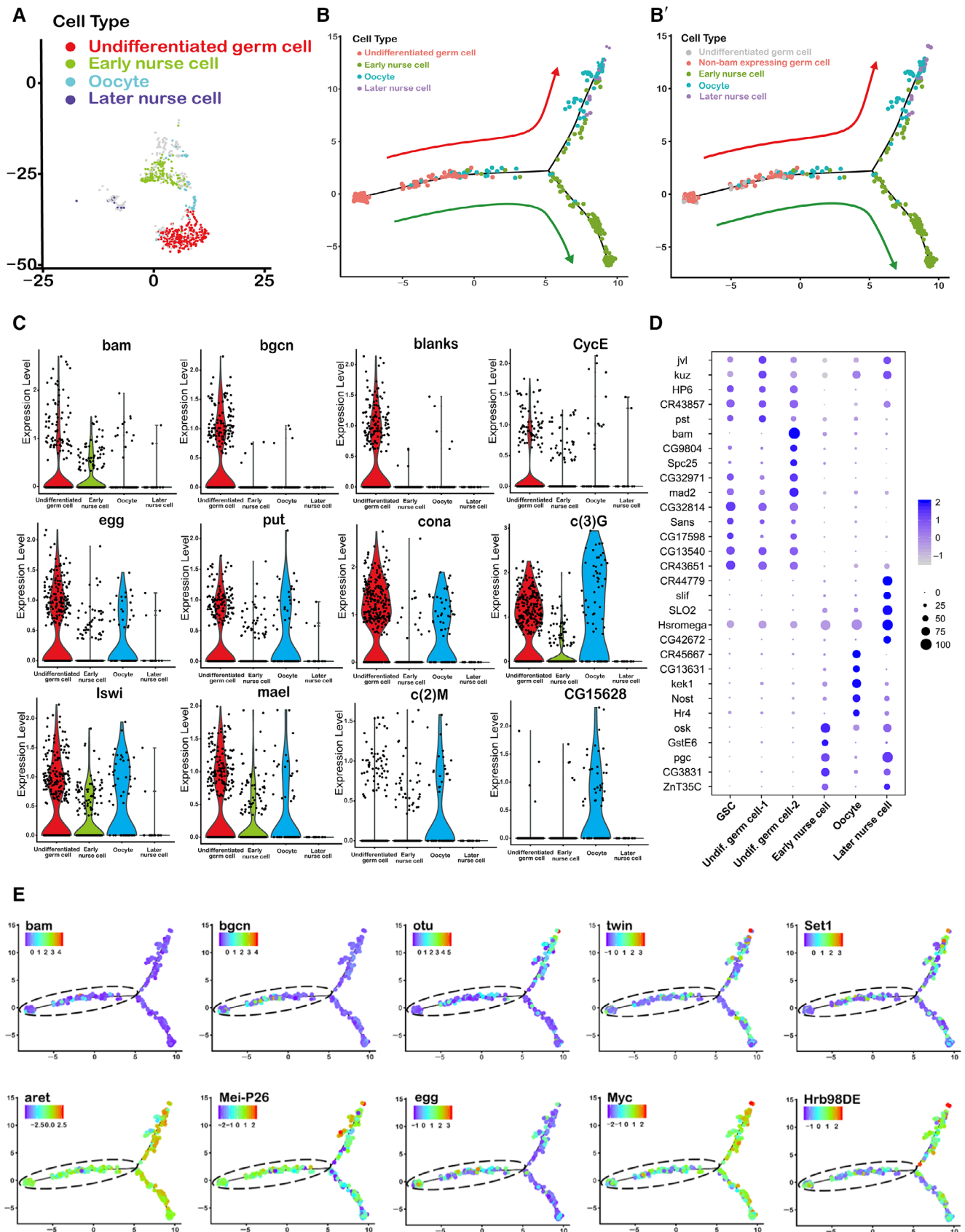


Figure 2.

**Figure 2. Identification of GSCs and germ cell subclusters.**

- A tSNE plot revealing four germ cell subclusters, undifferentiated germ cells (red), early nurse cells (green), oocytes (blue) and later nurse cells (purple).
- B, B' The Monocle analysis revealed the developmental linear trajectory of germ cells, and the putative GSCs population was distinguished in non-*bam* expressing germ cells which located in the beginning of trajectory. Arrows indicate the direction of differentiation.
- C To assign identities to these germ cell subclusters, the violin plots were used to visualize the distribution of normalized typical marker genes expression levels.
- D The dot plot presents the top 5 genes in the GSCs, undifferentiated germ cell-1, undifferentiated germ cell-2, early nurse cells, oocytes and later nurse cells. The dot diameter represents the percentage of cell expressing the indicated genes.
- E The expression of GSC maintenance genes (*aret*, *Mei-P26*, *egg*, *Myc* and *Hrb98DE*) and differentiation genes (*bam*, *bgcn*, *out*, *twin* and *Set1*) along the primary branch (dotted circle line) in pseudotime.

Source data are available online for this figure.

cent/post MB 8 were identified by *psd*, *Vml*, *ttk*, *dec-1*, *bond*, and *Fcp3C* (Jevitt et al, 2020a) at 0.5 resolution value ( $R = 0.5$ ). The MBFC (stg. 12) and MBFC (stg. 14) were easily identified by marker genes such as *Femcoat*, *Ilp8*, and *yellow-g* at 0.5 resolution value ( $R = 0.5$ ). The well-recognized marker genes *Hlm* and *su(r)* were used to identify hemocyte and plasmatocyte clusters, respectively (Jevitt et al, 2020a; Li et al, 2022).

### Identification of a GSC cluster and two distinct undifferentiated germ cell subpopulations

To refine our clustering results, the GSC differentiation-related markers, such as *bam*, *bgcn*, *blanks*, and *cycE* (Perinthottathil & Kim, 2011; Rust et al, 2020a), were used to identify undifferentiated germ cells, while *egg*, *put*, and *cona* were used to identify GSCs and oocytes (Xie & Spradling, 1998; Page et al, 2008; Clough et al, 2014). The enrichment of *c(3)G*, *Iswi*, and *mael* was observed in the undifferentiated germ cell cluster and the early nurse cell and oocyte clusters, and *CG15628* was observed specifically in the oocyte (Fig 2C).

To characterize the spatial and temporal changes in transcription that occurs during the initial stages of germ cell differentiation, we used Monocle3 to construct a developmental trajectory of the four germ cell clusters (Fig EV1C). This analysis produces a graph-based trajectory called pseudotime that predicts the transcriptomic changes along the putative timing of a developmental process (Witt et al, 2019). In this case, four germline clusters were arranged into a linear trajectory consisting of a stem with two branches, which is consistent with the specification of the nurse cell and oocyte fates downstream from the CB fate. We identified a subset of *bam*<sup>-</sup> cells at one end of the trajectory as GSCs (Fig 2B and B'), and we assigned the remaining non-*bam* expressing cells and *bam*-positive cells to two distinct undifferentiated germ cell subclusters, namely undifferentiated germ cell-1 and undifferentiated germ cell-2. To further investigate this hypothesis and examine the putative GSC cluster, we plotted the GSC-related gene expression in pseudotime. Similar expression profiles of functional GSC differentiation genes (*bam*, *bgcn*, *out*, *twin*, and *Set1*; Steinhauer & Kalfayan, 1992; Ohlstein et al, 2000; Fu et al, 2015; Vidaurre & Chen, 2021) and GSC maintenance genes (*aret*, *Mei-P26*, *egg*, *Myc*, and *Hrb98DE*; Rhiner et al, 2009; Ji & Tulin, 2012; Blatt et al, 2020; Rastegari et al, 2020; Casale et al, 2021) were revealed in the trajectory (Fig 2E). Consistent with our expectations, we observed low expression of genes associated with differentiation and high expression of genes associated with self-renewal, while their expression patterns along the trajectory were gradually changed over time. The

expression patterns of top five expressed genes in three germline subclusters suggested that the developmental states of cells in the GSC cluster and undifferentiated germ cell-1 cluster were similar to each other but different from that of the undifferentiated germ cell-2 cluster (Fig 2D).

### Construction of a gene regulatory network in GSCs

Although a large number of genes are expressed in all germ cells, some genes that are differentially expressed during early germ cell development may play a more important role in the specification or maintenance of GSC fate. To identify these types of genes, we conducted a comparative analysis of the transcriptional profile of six germ cell subclusters. We identified subsets of genes in the germline-1 and -2 clusters, the early nurse cell cluster, the oocyte cluster and the later nurse cell cluster, that are differentially expressed compared to the GSC cluster (Fig 3A). In addition, we performed an RNAi screen of 35 differentially upregulated genes in the GSCs vs. undifferentiated germline-1 and the GSCs vs. undifferentiated germline-2 clusters by using *nos-Gal4* to drive expression in germ cells and *tub-Gal80<sup>ts</sup>* to limit RNAi expression to the adult stage. We found that RNAi knockdown of 19 upregulated genes induced disruption of GSC/CB homeostasis. Of these, RNAi knockdown of 12 of the genes caused a change in the number of GSCs or CBs; RNAi knockdown of six genes caused a complete loss of GSCs and germ cells (an “empty germarium” phenotype); and RNAi knockdown of four genes caused a severe disruption of germ cell differentiation, as evidenced by an abnormal fusome structure (a “differentiation defect” phenotype). Notably, the knockdown of *CG2098* (*FeCH*) and *CG4858* (*Nubp2*) caused both changes in the number of GSCs or CBs and differentiation defects, and thus were counted in both categories. The knockdown of *CG3983* (*Ns1*) caused both changes in the number of GSCs or CBs and the empty germarium phenotype (Fig 3B and C, and Appendix Table S4). Lastly, we identified the differentially expressed genes (score > 980) and constructed an interaction network (Fig 3D). This analysis revealed a dense network of interactions between the differentially expressed genes, with genes that regulate translation (eIF2gamma, Ns1, and Prp19) forming major nodes. In addition, we found that RNAi knockdown of 20 out of the 37 most highly expressed genes also caused a significant increase or decrease in the number of GSCs or CBs per germarium. The knockdown of four genes could cause the differentiation defects, among which the knockdown of *CG8589* (*tejas*) and *chinmo* could cause the changes in the number of GSCs or CBs and differentiation defects. The knockdown of *CG8093* caused the empty germarium phenotype (Fig 2A and B, and Appendix Table S5).

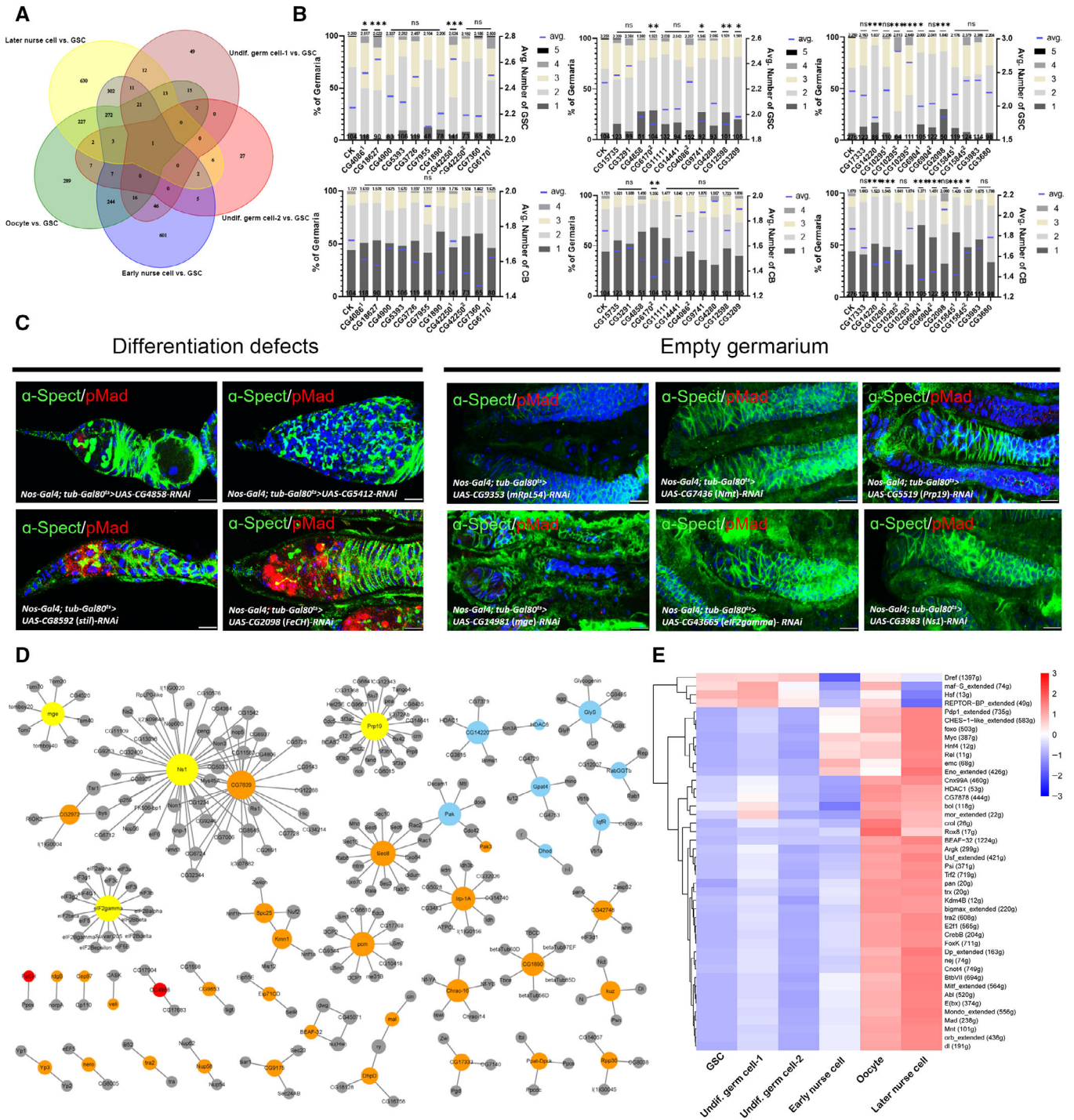


**Figure 3. Construction of the gene regulatory network in GSCs.**

A A Venn diagram of the number of genes that are differentially expressed between the indicated pairs of clusters.  
 B Statistical analysis of the average number of GSCs and CBs in RNAi lines of screened differentially expressed genes. The bars in blue show the mean value, one-way ANOVA, ns indicates no significant difference, \* $P < 0.05$ , \*\* $P < 0.01$ , \*\*\* $P < 0.001$ ,  $n \geq 65$ , biological replicates. Note, superscripts indicate different RNAi lines of the same gene (CG4806, CG42250, CG6170, CG10295, CG6904 and CG15845) used in RNAi screening experiment.  
 C The typical phenotypes of germlaria in selected RNAi lines stained with anti- $\alpha$ -Spectrin (green) and anti-pMad (red). The scale bar is 10  $\mu$ m.  
 D The gene interaction network predicted by Cytoscape v3.9.1.  
 E The heat map of SCENIC analysis of the GSC, undifferentiated germ cell-1, undifferentiated germ cell-2, early nurse cell, oocyte and later nurse cell subclusters.

Source data are available online for this figure.

To identify the transcription factor-based gene regulatory network in different kinds of germ cells, we applied SCENIC analysis to our single-cell RNA sequencing data with 6 known germ cell types. The analysis revealed that the Dref, mal-f, Hsf, and REPTOR-BP regulons were enriched in the GSC cluster, suggesting that they may play an important role in the regulation of early GSC development (Fig 3E). GO and KEGG enrichment analysis provided additional information about the biological processes that are enriched during germ cell development. Specifically, we found that the enriched GO terms included several that refer to processes in basic cell physiology such as “cellular metabolic process”, “protein catabolic process,” “cytoskeleton organization,” and “cell cycle” (Fig EV2C). The top 10 pathways in the KEGG enrichment analysis revealed that the differentially expressed genes in GSC, undifferentiated germ cell-1 and -2 clusters were significantly enriched for DNA replication and disease related pathways, and only early nurse cell cluster was enriched in the genes that are part of the ribosome category (Fig EV2D).

### Validation of candidate marker genes in germ cells

To identify new markers of distinct stages of germ cell differentiation, we selected 10 candidate genes that are predicted to be expressed in GSCs by pseudotime analysis and assayed their expression patterns by *in situ* hybridization. These included nine GSC-specific markers and one marker of germline cysts (Fig 4A). We identified seven genes that were specifically expressed in the anterior tip of the germarium, where the GSCs are located, including one gene, CG32814, which we named *eggplant* (*eggpl*) because knockdown causes an enlarged ovary with many retained eggs, as described below (Fig 4B). To validate the expression patterns at the protein level, we generated antibodies against two proteins, the basal transcription factor TflIA-S (Andersen et al, 2017) and Eggpl which contains 244 amino acids (predicted molecular weight of 27.2 KD). The primary amino acid sequence of Eggpl contains a large intrinsically disordered region (IDR) that aligns with *Drosophila* and mammalian mucins (Appendix Fig S3), which are secreted proteins. However, the *eggpl* sequence does not contain any signal peptides or transmembrane regions, suggesting that it may function in the cytoplasm (Fig EV3A). Consistent with the bioinformatic predictions and *in situ* hybridization results, we found that the immunofluorescence signals of both antibodies were highly enriched in GSCs and early germ cells (Fig 4C and E). We also validated the efficacy of anti-Eggpl by generating a knock-in (KI) line in which the endogenous *eggpl* allele is tagged with GFP (*eggpl::GFP*; Fig EV3B) and double staining for Eggpl and GFP (Fig EV4). Both TflIA-S and Eggpl were localized to the cytoplasm, which we confirmed *in vitro* using the Sf9 cell line (Fig 4F). In addition to these genes with highly specific expression patterns, we also found that *hang*, a conserved regulator of ethanol tolerance (Scholz et al, 2005), was expressed in germ cells throughout the germarium, and that CG7255 was expressed in germ cell cysts and nurse cells but not in GSCs. These expression patterns also aligned with the order of expression of *eggpl*, *hang*, and CG7255 predicted by pseudotime analysis (Fig 4D).

### The unique expression patterns of *eggpl* in the germline

To further characterize the cells that express *eggpl*, we colabeled for *eggpl* mRNA and either  $\alpha$ -Spectrin protein, which localizes to a

cytoplasmic structure that is spherical in GSCs (called “spectrosomes”) and elongates to “fusomes” in cystoblasts (Xie & Spradling, 2001), or the germ cell-specific protein, Vasa (Fig 5A and B). We found that *eggpl* mRNA was specifically enriched in GSCs and CBs (Fig 5C). To confirm this observation, we probed for *eggpl* in a *bam::GFP* line. Indeed, we found that *eggpl* transcript was enriched in the *Bam::GFP*<sup>+</sup> cells at the anterior tip of the germarium, consistent with GSC specific expression (Fig 5E).

To assess the pattern of Eggpl protein expression, we costained *eggpl::GFP* for GFP and  $\alpha$ -Spectrin, pMad (Fig 5D), or anti-Bam (Fig 5G) and found that Eggpl::GFP was detectable in germ cells throughout Region 1 (Fig 5D). Interestingly, Eggpl::GFP protein levels varied by stage, with the highest level of expression in the cells just downstream from the GSC niche (Fig 5J and N). Further, to directly determine whether *eggpl* transcripts and Eggpl protein consistently expressed in anterior germarium, we simultaneously performed *in situ* hybridization and immunostaining of Eggpl in the *eggpl* knock-in line. The result of double staining showed that the *eggpl in situ* signal aligned well with the GFP signal, which indicated that *eggpl* marks the GSCs and CBs in germarium at both the transcriptional and protein levels (Fig 5I). In addition, we constructed a *UAS-eggpl-GFP* line and examined the overexpression pattern of *eggpl* by using mRNA *in situ* hybridization (Fig 5F and H). We observed broad expression of *eggpl* in Region 1 of the overexpression line. Together, these results suggest that the *eggpl* gene expression is consistent at the mRNA and protein levels.

### Ectopic expression of *eggpl* affects the differentiation of germline stem cells and cystoblasts

To determine whether *eggpl* is involved in the regulation of GSC fate, we expressed *UAS-eggpl-RNAi* and *UAS-eggpl-GFP* lines with *nos-Gal4* and used *tub-Gal80<sup>ts</sup>* to provide temporal control. We raised flies at 18°C to inhibit Gal4 activity and then shifted adults to 29°C for 7 days, dissected ovaries and stained for pMad and  $\alpha$ -Spectrin to identify GSC and early germ cells (Fig 5K). With this combination of markers, GSCs were identified as cells at the tip of the germarium that have high levels of pMad and spherical  $\alpha$ -Spectrin<sup>+</sup> spectrosomes, whereas the differentiating germline cysts (2-, 4-, 8-, and 16-cell) as cells were identified by the low levels of pMad and the presence of  $\alpha$ -Spectrin<sup>+</sup> branched fusomes (Xie & Spradling, 2001). Upon knockdown of *eggpl*, we did not observe a significant difference in GSC or CB number but found a significant increase in cysts at the 2-cell and 4-cell stages (Fig 5L and M). To further study *eggpl* function, we generated an *eggpl* allele, *eggpl<sup>l1</sup>*, using CRISPR. Immunostaining with the anti-Eggpl antibody was undetectable in *eggpl<sup>l1</sup>* germaria (Fig 5O), indicating that the allele disrupts protein expression. Consistent with our RNAi results, both the number of GSCs and the number of CBs were not affected in *eggpl<sup>l1</sup>*, while the number of germline cysts in the 2-cell to 8-cell stages was significantly increased (Fig 5P and Q). To determine whether the depression of *eggpl* affects germ cell apoptosis, we performed a TUNEL assay and caspase-3 staining on *eggpl-RNAi* and *eggpl<sup>l1</sup>* lines. We found that the average number of apoptotic germ cells was not affected by RNAi knockdown of *eggpl* (Fig 5R). Taken together, these results indicate that *eggpl* is required for early germ cell differentiation but is likely dispensable for maintaining germ cell survival at these stages.

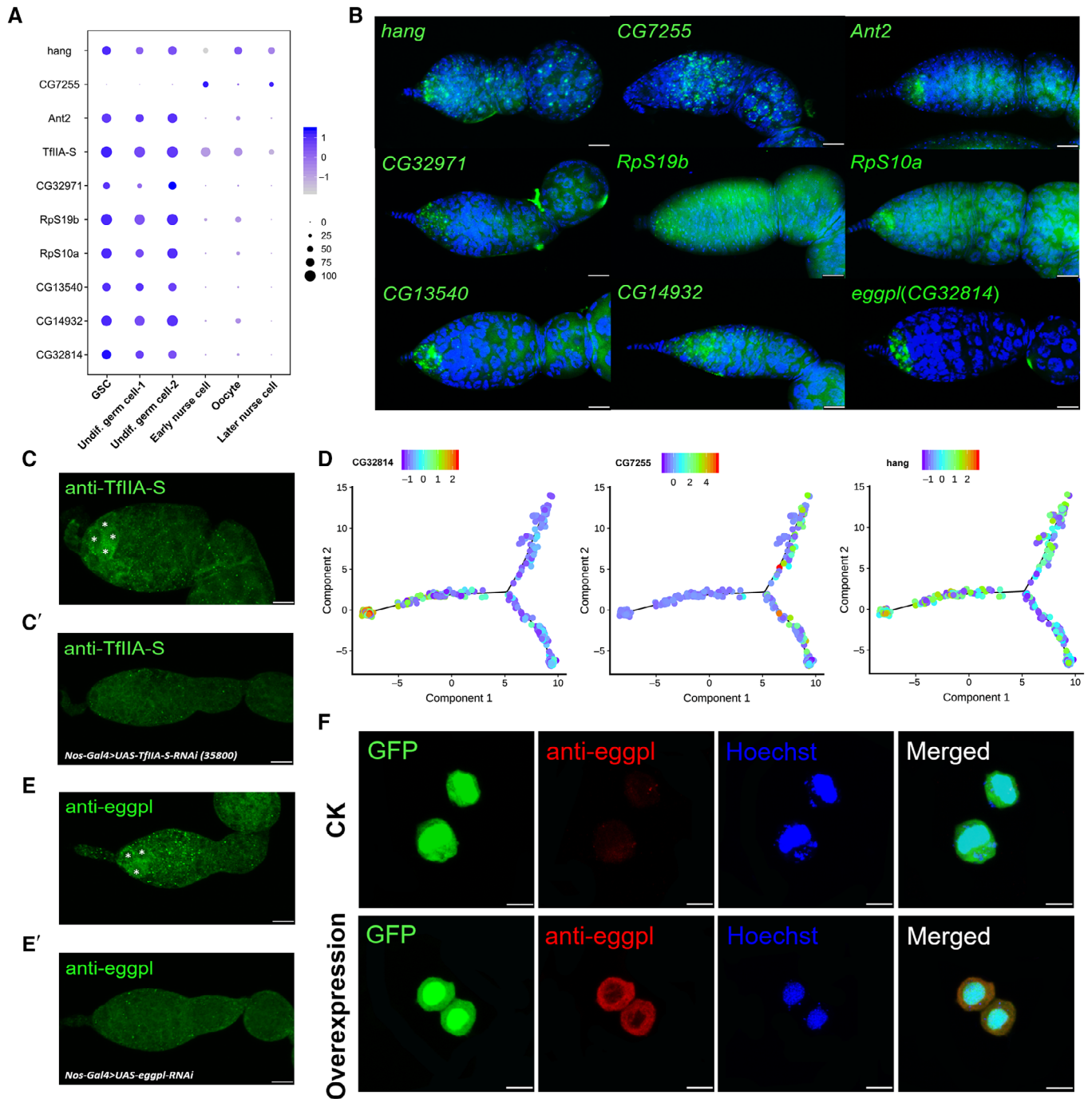


**Figure 4. Validation of GSC marker genes.**

- A** A dot plot showing the expression of selected specific marker genes in each subcluster. The color intensity from dark to light represents the average normalized gene expression level.
- B** The expression patterns of candidate marker genes were validated by using *in situ hybridization*. The scale bar is 10  $\mu$ m.
- C, C'** Immunofluorescence staining with anti-TfIIA-S on wild type and *nos-Gal4 > UAS-TfIIA-S-RNAi* (negative control). The scale bar is 10  $\mu$ m.
- D** The expression profiles of *eggpl*, *CG7255* and *hang* along the trajectory branches in pseudotime.
- E, E'** Immunofluorescence staining with anti-eggpl on wild type and *nos-Gal4 > UAS-eggpl-RNAi* (negative control) ovary. The scale bar is 10  $\mu$ m.
- F** The overexpression of GFP (green) and *eggpl* in Sf9 cell line *in vitro*. The anti-eggpl (red) was used to detect the eggpl protein, and Hoechst (blue) was used to label the nucleus. The scale bar is 10  $\mu$ m.

Source data are available online for this figure.



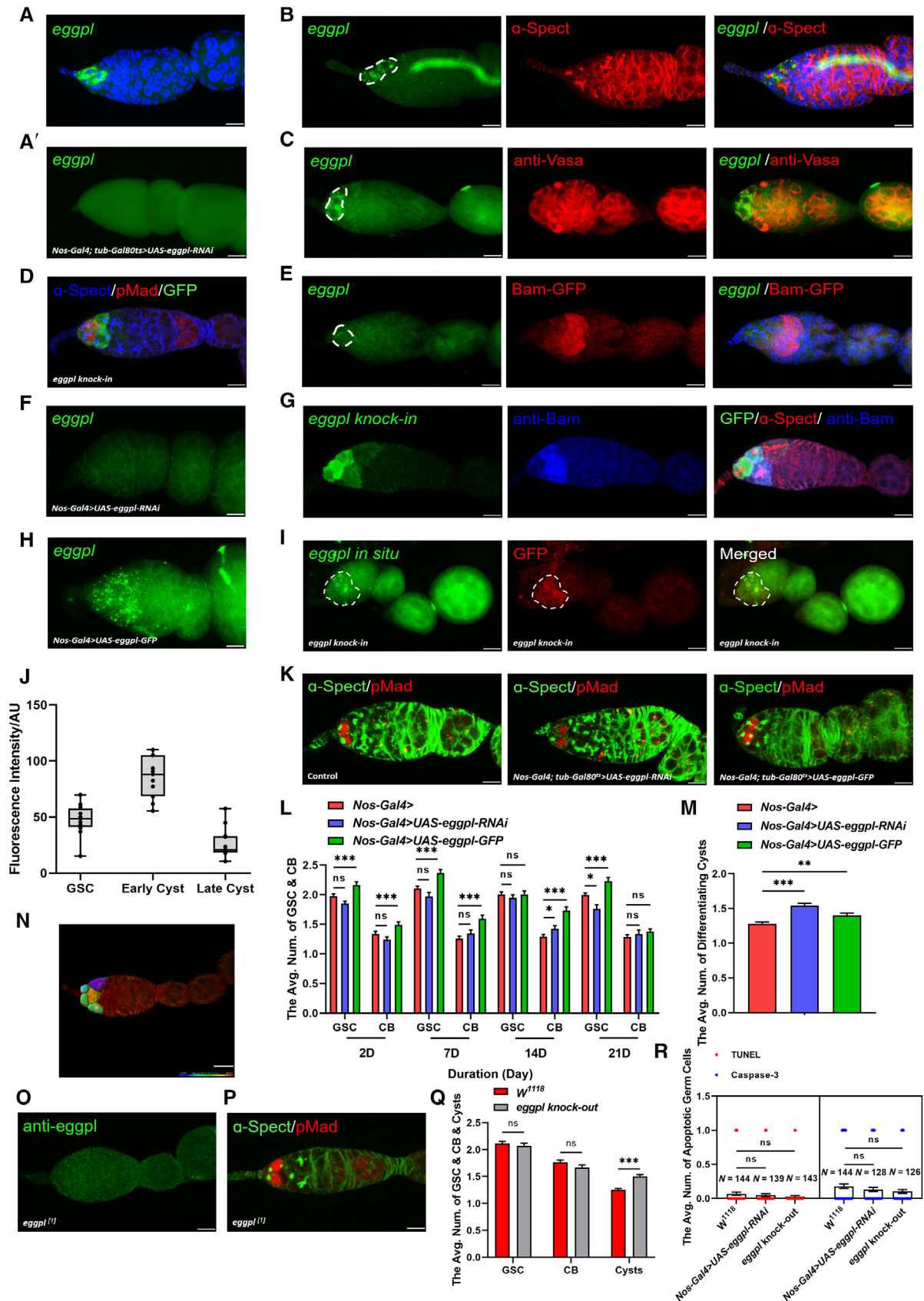
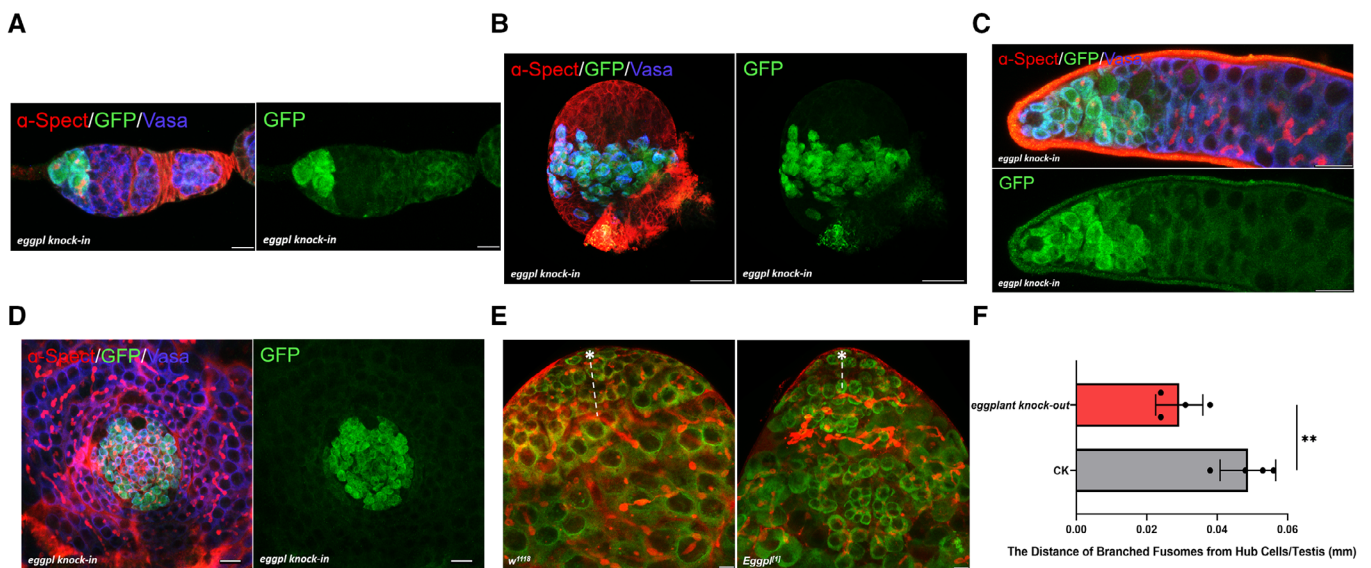


Figure 5.

**Figure 5. The characteristics of *eggpl* expression in the ovarian germline.**

- A, A' The mRNA *in situ* hybridization of *eggpl* (green) on wild type and *nos-Gal4 > UAS-eggpl-RNAi* (negative control) line. The scale bar is 10  $\mu$ m.
- B, C Immunofluorescence staining with anti- $\alpha$ -Spectrin (red) and anti-Vasa (red) on *eggpl-in situ* (green) labeled tissues respectively. The scale bar is 10  $\mu$ m. The dashed line indicates the *eggpl-in situ* (green) signals.
- D Immunofluorescence staining with anti- $\alpha$ -Spectrin (blue), anti-pMad (red) and GFP (green) on the *eggpl::GFP knock-in* line. The scale bar is 10  $\mu$ m.
- E The mRNA *in situ* hybridization of *eggpl* (green) on *bam::GFP* line stained with GFP (red). The scale bar is 10  $\mu$ m. The dashed line indicates the *eggpl-in situ* (green) signals.
- F–H (F, H) The mRNA *in situ* hybridization of *eggpl* (green) on *nos-Gal4 > UAS-eggpl-RNAi* (negative control) (F) and *nos-Gal4 > UAS-eggpl-GFP* lines (H). The scale bar is 10  $\mu$ m. (G) The anti-GFP, anti- $\alpha$ -Spectrin (red) and anti-Bam (blue) were used to stain on *eggpl::GFP knock-in* line. The scale bar is 10  $\mu$ m.
- I Double staining with *eggpl in situ* and anti-GFP on *eggpl knock-in* lines. The scale bar is 10  $\mu$ m. The dashed line indicates the *eggpl-in situ* (green) signals.
- J Quantification of the GFP intensity mean in *eggpl::GFP knock-in* line (biological replicates,  $n = 11$ ). The central band indicates the median, the box length indicates the interquartile range, and the upper and whisker indicate the maximum and minimum value respectively.
- K The phenotypes of wild type, *nos-Gal4 > UAS-eggpl-RNAi* line and *nos-Gal4 > UAS-eggpl::GFP* line staining with anti- $\alpha$ -Spectrin (green), anti-pMad (red). The scale bar is 10  $\mu$ m.
- L The average number of GSC and CB in *nos-Gal4* line, *nos-Gal4 > UAS-eggpl-RNAi* line and *nos-Gal4 > UAS-eggpl::GFP* line on 2, 7, 14 and 21 day. Error bars show mean  $\pm$  SEM, one-way ANOVA, ns indicates no significant difference,  $*P < 0.05$ ,  $***P < 0.001$ ,  $n \geq 72$ , biological replicates.
- M The average number of differentiating germline cysts in three types of fly lines. Error bars show mean  $\pm$  SEM, one-way ANOVA,  $**P < 0.01$ ,  $***P < 0.001$ ,  $n \geq 261$ , biological replicates.
- N Image illustrating the image segmentation used to quantify the expression pattern of *eggpl*. The scale bar is 10  $\mu$ m.
- O Immunofluorescence staining of an *eggpl<sup>121</sup>* germlarium with anti-*eggpl* antibody showing a lack of signal. The scale bar is 10  $\mu$ m.
- P The typical phenotype of *eggpl<sup>121</sup>* germlarium staining with anti- $\alpha$ -Spectrin (green), anti-pMad (red). The scale bar is 10  $\mu$ m.
- Q The statistical analysis of the average number of GSCs and CBs and Cysts in *eggpl<sup>121</sup>* line. Error bars show mean  $\pm$  SEM, one-way ANOVA, ns indicates no significant difference,  $***P < 0.001$ ,  $n \geq 104$ , biological replicates.
- R The average number of apoptotic germ cells in wild type, *nos-Gal4 > UAS-eggpl-RNAi* line and *eggpl<sup>121</sup>* line. Error bars show mean  $\pm$  SEM, one-way ANOVA, ns indicates no significant difference (biological replicates,  $n = 3$ ), and  $N$  represents the total number of counted ovarioles.

Source data are available online for this figure.

**Figure 6. *Eggpl* is dynamically expressed in testis and ovary.**

- A Immunofluorescence staining with anti- $\alpha$ -Spectrin (red), anti-Vasa (blue) and anti-GFP (green) on adult ovary. The scale bar is 10  $\mu$ m.
- B Immunofluorescence staining on PGCs of larvae ovary. The scale bar is 20  $\mu$ m.
- C Immunofluorescence staining on GSCs and early spermatogonia in adult testis. The scale bar is 20  $\mu$ m.
- D Immunofluorescence staining on PGCs of larvae testis tissue. The scale bar is 20  $\mu$ m.
- E Immunofluorescence staining with anti- $\alpha$ -Spectrin (red) and anti-Vasa (green) on testis from wild type or *eggpl<sup>121</sup>* flies. The scale bar is 10  $\mu$ m.
- F The measurement of distance between hub cells and early germ cyst (biological replicates,  $n = 4$ ), error bars show mean  $\pm$  SEM, two-tailed Unpaired Student's *t*-test,  $**P < 0.01$ .

Source data are available online for this figure.

### Expression of *eggpl* in GSCs and primordial germ cells in both the ovary and testis at different developmental states

Many genes regulate germ cell differentiation in both males and females, and, indeed, we found that *eggpl* is also expressed in both

female and male GSCs and early spermatogonia (Fig 6A and C). Since the *Drosophila* GSCs are derived from a small population of primordial germ cells (PGCs) with undifferentiated states, the profiles of gene expression in PGCs may vary from that of the adult. To detect whether *eggpl* is also expressed in germ cells prior to

adulthood, we dissected the gonads from male and female larvae in *eggpl* knock-in lines, and stained with anti- $\alpha$ -Spectrin and anti-Vasa to label the PGCs and germ cells. We found that *eggpl* expressed in both male and female larvae PGCs and early undifferentiated germ cells (Fig 6B and D), suggesting that *eggpl* may function at these early stages as well. In the testes of wild-type male flies, GSCs are present next to the apical tip of testes and gradually differentiate into spermatogonial cells with germline-specific branched fusomes. We found that the average distance of branched fusomes from the hub cells in *eggpl* knock-out testes was significantly less than in testes from control flies (Fig 6E and F). This finding suggests that GSCs in the testes differentiate prematurely when *eggpl* is lost.

### Depression of *eggpl* expression increases egg production and regulates germ cell proliferation

Since the disruption of *eggpl* led to an increase in the frequency of germ cell cysts, we examined the rate of oviposition in *eggpl*-RNAi and *eggpl*<sup>l1</sup> lines, and found a significant increase in the number of eggs laid by both lines compared to controls (Fig 7B). In addition, we noticed that the size of the whole ovary and the number of mature eggs per ovary were substantially increased upon RNAi knockdown or knock out of *eggpl* in germ cells at 2-, 7-, and 14-day-old flies but returned to a size that is comparable to wildtype by 21-days (Fig EV3B). Based on this phenotype, we named the gene *eggplant*. We surmised that *eggpl* could be involved in the regulation of proliferation. To test this possibility, we assayed for germ cell proliferation using a BrdU incorporation assay, which labels cells in S-phase, and by staining for phosphor-histone H3 (PH3), which labels cells in mitosis (Fig 7A and C). Compared with wild type flies fed a standard diet, the average number of BrdU<sup>+</sup> cysts was significantly increased in germlaria from wild type flies fed on rich yeast diet, *eggpl*-RNAi flies fed a standard or a rich diet, and *eggpl*<sup>l1</sup> flies fed a standard or a rich diet (Fig 7D). Furthermore, we found that the average number of PH3<sup>+</sup> germ cells was significantly increased in *eggpl* knockdown and knock-out lines (Fig 7E). These results suggest that the depression of *eggpl* expression may accelerate the proliferation rate of germ cells.

The increase in ovary size and GSC proliferation rate that we observed upon knockdown of *eggpl* phenocopies the response of ovaries to a rich protein diet (i.e., daily feeding of wet yeast paste). This suggests that the wet yeast diet may be promoting oogenesis in part by repressing *eggpl* expression. To test this hypothesis, we compared the ovaries from control and *eggpl*<sup>l1</sup> flies that were maintained on standard food or a rich diet of standard food plus wet yeast paste. The ovary size of the control flies was substantially increased by the addition of wet yeast paste, consistent with previous reports (Drummond-Barbosa & Spradling, 2001). Interestingly, we found that the ovary size and the number of mature eggs in *eggpl* knockout lines maintained on standard food increased rapidly after eclosion and, by 7 days, were significantly higher than wild type controls fed a standard diet. The ovary size and number of mature eggs per ovary of the *eggpl* knockout flies maintained on a rich diet also increased rapidly after eclosion and, by 14 days, exceeded the values we observed in wild type flies maintained on a rich diet (Fig 7H–K). In addition, we found that the intensity of *eggpl* signal was significantly decreased in flies that were maintained with wet yeast paste (Fig 7F and G). Taken together, these observations

suggest that *eggpl* is an intrinsic signal in germ cells that helps to translate nutritional cues into the regulation of germ cell proliferation and the rate of oogenesis.

### PI3K regulates the expression of *eggpl*

Wet yeast paste in the diet promotes increased egg production by signaling to the GSC niche through the insulin pathway. Therefore, we hypothesized that *eggpl* is regulated by insulin signaling in the early GSC lineage. To test this hypothesis, we modulated the activity of PI3K, which is a positive regulator of the insulin signaling pathway, functioning just downstream of the receptor. Specifically, we expressed either the constitutively active form (*Dp110*<sup>CA</sup>) or the dominant negative form (*Dp110*<sup>DN</sup>) of the catalytic subunit of PI3K using *Nos-Gal4* and then assayed for germ cell proliferation and *eggpl* expression. Insulin signaling stimulates germ cell proliferation and, indeed, we observed that overexpression of the *Dp110*<sup>CA</sup> allele or the *Dp110*<sup>DN</sup> allele caused an increase or decrease in the number of BrdU<sup>+</sup> cysts, respectively, as expected. Likewise, feeding flies a rich diet increased the number of BrdU<sup>+</sup> cysts for all genotypes. Interestingly, we observed that the reduction in the number of BrdU<sup>+</sup> cysts upon overexpression of *Dp110*<sup>DN</sup> was suppressed by knockdown of *eggpl* by RNAi (Fig 8A), indicating that *eggpl* is genetically downstream of PI3K in the regulation of germ cell proliferation. Furthermore, we found that Eggpl protein levels were significantly increased upon overexpression of *Dp110*<sup>DN</sup> and decreased upon overexpression of *Dp110*<sup>CA</sup> with either a standard or a rich diet (Fig 8B and C), indicating that Eggpl expression is regulated by PI3K. Collectively, these results support a model in which *eggpl* mediates the GSC differentiation process via insulin signaling pathway (Fig 8D). However, overexpression of *Dp110*<sup>CA</sup> caused a larger increase in the rate of BrdU incorporation than knockdown of *eggpl*, suggesting that activation of insulin signaling with this allele also affects other targets that regulate the cell cycle aside from just *eggpl*.

## Discussion

Decades of research have established the *Drosophila* female germline stem cell as a favorable system to understand germ cell and stem cell biology. The GSCs are required in germlarium to support continuous production of differentiating germ cells throughout most of adulthood. The GSCs are typically identified by their localization at the anterior tip of the germlarium (Shi et al, 2021), and the presence of spectrosomes or high pMad-signal (Xie, 2013; Fig 1B'), and many other useful marker genes have also been described. For example, the expression of *Lamin C*, a typical marker, is strongly expressed in TF cells, displays the weak expression in cap cells, and is not detectable in ECs. Conversely, *traffic jam* (*tj*) is highly expressed in ECs and cap cells, but not detectable in TF cells (Panchal et al, 2017). These markers facilitate many tissue- and cell type-specific genetic manipulations *in vivo*, which can be used to understand the gene functions and signaling pathways that regulate germ cell differentiation. Therefore, discovery of specific marker genes in GSCs will have many applications in the study of germ cell and stem cell biology. However, it has been difficult to identify new markers of GSCs, in part because they are rare in wildtype tissue,

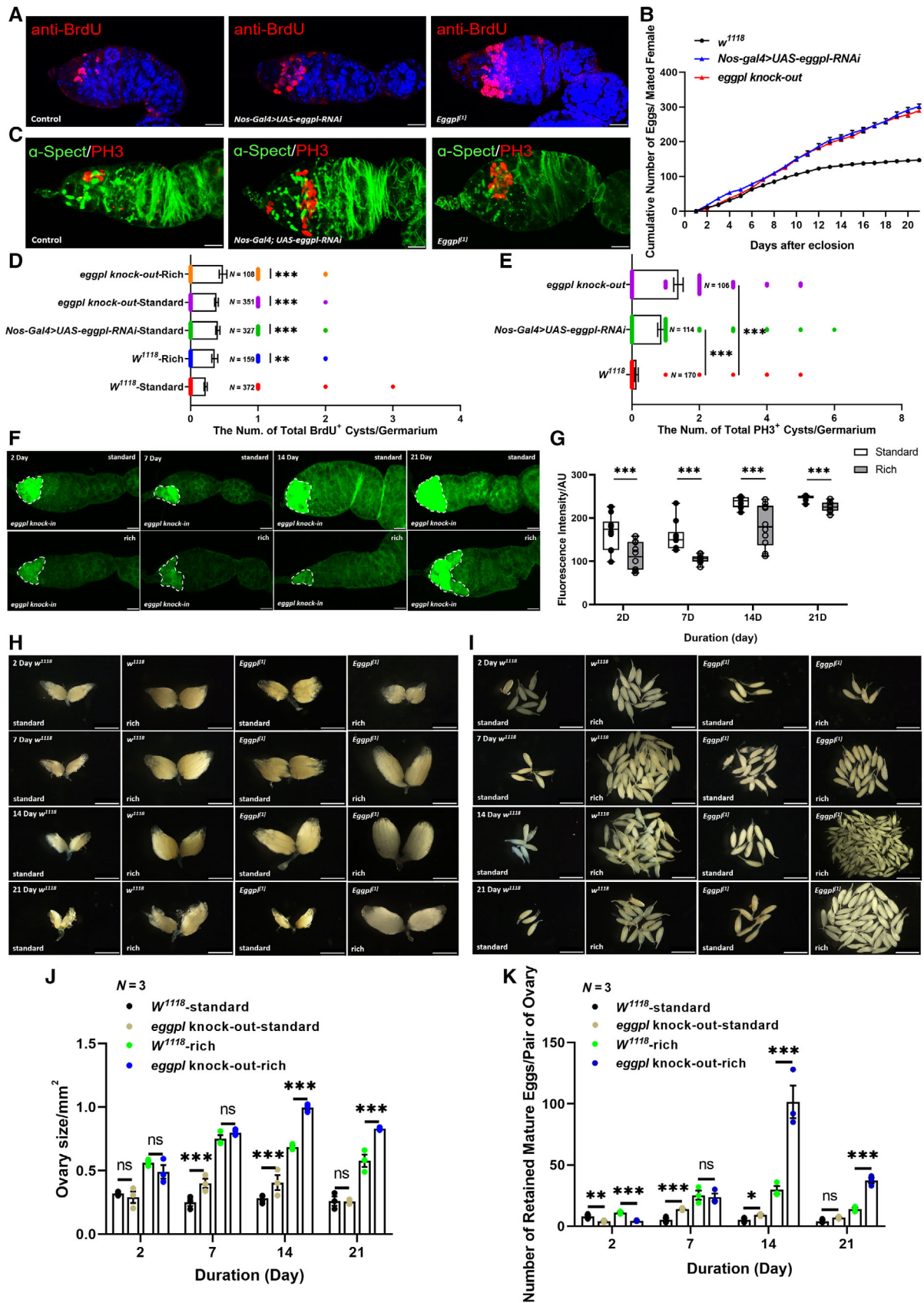
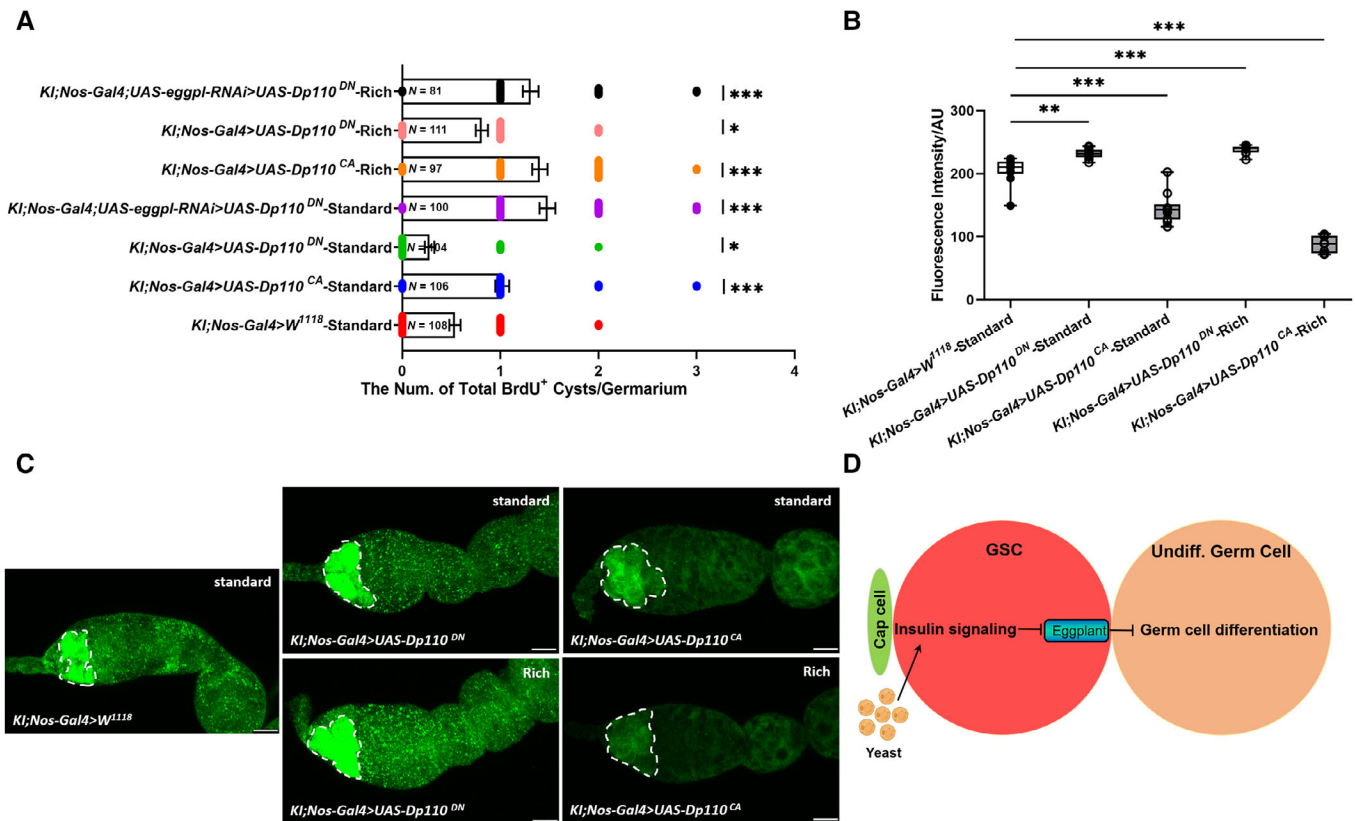


Figure 7.

**Figure 7. *Eggl* might be involved in the regulation of cell cycle of germline cysts.**

A Immunofluorescence staining with anti-BrdU (red). The scale bar is 10  $\mu$ m.  
 B The oviposition of wild type, *Nos-Gal4 > UAS-eggl-RNAi* and *eggl<sup>2J</sup>* line over 21 days. Error bars show mean  $\pm$  SEM, three biological replicates ( $n = 3$ ) were performed, and there were ten female and five male adult flies in each biological replicate.  
 C Immunofluorescence staining with anti- $\alpha$ -Spectrin (green) and anti-PH3 (red). The scale bar is 10  $\mu$ m.  
 D The number of BrdU<sup>+</sup> germ cell cysts. Error bars show mean  $\pm$  SEM, one-way ANOVA, \*\* $P < 0.01$ , \*\*\* $P < 0.001$ .  $N$  represents the total number of counted ovarioles.  
 E The number of PH3<sup>+</sup> germ cell cysts. Error bars show mean  $\pm$  SEM, one-way ANOVA, \*\*\* $P < 0.001$ .  $N$  represents the total number of counted ovarioles.  
 F Immunofluorescence staining with anti-GFP on germaria from *eggl::GFP knock-in* flies with or without feeding fresh yeast paste on day 2-, 7-, 14- and 21. The dotted line indicates the examined area. The scale bar is 10  $\mu$ m.  
 G Quantification of the GFP intensity mean in the *eggl::GFP knock-in* line. The central band indicates the median, the box length indicates the interquartile range, and the upper and whisker indicate the maximum and minimum value respectively. The 10 biological replicates ( $n = 10$ ) were performed, one-way ANOVA, \*\*\* $P < 0.001$ . The dashed line indicates the examined area.  
 H, I Images of ovaries or mature eggs from flies of the indicated genotypes, feeding conditions, and days post-eclosion showing comparisons of the overall ovary sizes (F) and the numbers of retained matured eggs (C). The scale bar is 500  $\mu$ m.  
 J, K Quantitative analysis of the ovary size (H) and the number of retained mature eggs (I) under different food conditions. Error bars show mean  $\pm$  SEM, one-way ANOVA, ns indicates no significant difference, \* $P < 0.05$ , \*\* $P < 0.01$ , \*\*\* $P < 0.001$ . The three biological replicates ( $n = 3$ ) were performed.  
 Source data are available online for this figure.



**Figure 8. Genetic interaction between *eggl* and the insulin signaling pathway.**

A The number of BrdU<sup>+</sup> germ cell cysts. Error bars show mean  $\pm$  SEM, one-way ANOVA, \* $P < 0.05$ , \*\*\* $P < 0.001$ .  $N$  represents the total number of counted ovarioles.  
 B Quantification of the GFP signal in germaria from *eggl::GFP knock-in* flies of the indicated genotypes under different conditions. The central band indicates the median, the box length indicates the interquartile range, and the upper and whisker indicate the maximum and minimum value respectively, one-way ANOVA, \*\* $P < 0.01$ , \*\*\* $P < 0.001$ ,  $n = 10$ , biological replicates.  
 C Immunofluorescence staining with anti-GFP on germarium with or without feeding fresh yeast paste on 7<sup>th</sup> day. The dashed line indicates the examined area. The scale bar is 10  $\mu$ m.  
 D Model depicting the regulation of *eggl* expression and its role in GSC differentiation.  
 Source data are available online for this figure.

and thus not amenable to bulk sequencing approaches. In our study, we performed single-cell RNA sequencing on whole ovaries and identified 24 distinct cell populations by using known marker genes

(Fig 1C and D). Our dataset aligns well with other published fly ovary datasets (Rust et al, 2020a; Data ref: Rust et al, 2020b; Jevitt et al, 2020a; Data ref: Jevitt et al, 2020b; Slaidina et al, 2021; Data

ref: Slaidina & Lehmann, 2021; Li et al, 2022) and has a similar number of cells (Appendix Fig S1). Three of the four other studies used a  $w^{1118}$  background, as we did (Appendix Table S2). Notably, our dataset had a substantially higher percentage of germ cells than the Rust et al or Jevitt et al datasets (5.2% vs. 1.3% and 1.6%, respectively) and was similar to the Slaidina et al dataset (6.9%) but much less than the Fly Cell Atlas (12.6%; Appendix Fig S2). These differences may be due to variation in the sample preparation methods. Here, we analyzed the 175 cells in the GSC cluster to identify individual genes and gene regulatory networks that may be important for GSC function. This approach produced a list that is highly enriched for genes that produce a phenotype when knocked down in germ cells by RNAi or that have a specific expression pattern in the early GSC lineage. This validates the approach and provides a new resource for the community.

The evolutionarily conserved insulin-like growth factor pathway has multiple roles in the modulation of GSC proliferation and maintenance. A protein-rich diet induces the production of insulin-like peptides (DILPs) in the brain, which regulate GSC division and cyst growth on a protein-rich diet (LaFever & Drummond-Barbosa, 2005). Several intracellular signals have been identified that function downstream of insulin signaling in germ cells. These include phosphoinositide-3 kinase (*Dp110*), *dFOXO*, and cell cycle factors, such as *CycA*, *CycB*, *CycE*, and *E2F1* (Hinnant et al, 2017; Kahney et al, 2019). However, little is known about the gene targets of this pathway that modulate the rate of differentiation. Here, we found that knockdown or knockout of *eggpl* mimics the effects of a rich yeast diet on the rate of BrdU incorporation, ovary size, and the number of retained eggs (Fig 7H–K). In addition, we found that either a rich yeast diet or overexpression of a constitutively active allele of *Dp110* causes a decrease in *eggpl* expression (Fig 7F–I), and that *eggpl* knockdown was epistatic to *Dp110<sup>DN</sup>* expression, reversing its negative effects on the rate of BrdU incorporation. Taken together, these observations suggest that *eggpl* functions as a negative regulator of oogenesis downstream of insulin signaling (Fig 8D). However, we did not test other components of the insulin pathway in this study, and *eggpl* is not among the genes that have been identified as direct targets of the canonical insulin pathway transcription factor, *foxo* in chromatin immunoprecipitation (ChIP) preparations from whole adult flies (Alic et al, 2011), so the mechanism by which *eggpl* expression is regulated by the insulin pathway is not fully resolved. For example, it may be that PI3K regulates *eggpl* expression independently of *foxo* or that *eggpl* is regulated by insulin signaling indirectly (e.g., downstream of a direct target of *foxo*). Alternatively, it may be that *eggpl* is a direct target of *foxo* but other factors limit its expression to a small number germ cells, and thus it was not detected in ChIP preparations from whole flies. Future studies investigating the interaction between *eggpl* and both other components of the insulin pathway as well as related genes may help to resolve these possibilities.

Although *eggpl* expression has been detected in other genomic studies of the ovary (Rust et al, 2020a; Tarikere et al, 2022), to our knowledge, this is the first study to investigate the *eggpl* expression pattern *in vivo* and the phenotype of *eggpl* mutants. It remains unclear how *eggpl* regulates oogenesis downstream of insulin signaling, but its similarity to mucins raises the interesting possibility that it may function as a cell signaling component (Singh & Hollingsworth, 2006). It is interesting that knockdown or knockout of *eggpl*

is sufficient to induce such a substantial increase in egg laying on standard food without yeast supplementation (Fig 7B). This suggests that protein in the diet is not initially a limiting factor under these conditions. Consistent with the increased egg laying phenotype, *eggpl<sup>11</sup>* flies also developed larger ovaries by 7 and 14 days of maintenance on a standard diet. However, *eggpl<sup>11</sup>* ovaries returned to a similar size as the control by 21 days (Fig 7J), suggesting that the ability of the *eggpl* knockout to phenocopy the rich diet under standard conditions cannot be sustained long term, perhaps due to energetic constraints.

Taken together, our research unveiled several new features of the early GSC lineage. The dataset we generated will be a valuable resource for future studies of germ cell biology. In addition, our functional studies demonstrate the utility of this resource and add to the understanding of how oogenesis is regulated by external cues.

## Materials and Methods

### Fly stocks and fly husbandry

The gene names, genetic symbols, and detailed information about fly strains applied in this study are presented in the text and in FlyBase. All fly stocks were maintained at 25°C and reared on standard cornmeal agar food. The following flies were used in this study:  $y^1w^{1118}$ , *nos-Gal4/CyO;tub-Gal80<sup>ts</sup>/TB*, *vasa-EGFP*, *nos-Gal4*, *UAS-Dp110<sup>DN</sup>*, and *UAS-Dp110<sup>CA</sup>* (gifts from Suning Liu, South China Normal University, China), *bam::GFP* (a gift from Yu. Cai, Temasek Life Sciences Laboratory, Singapore).

The RNAi fly lines were obtained from Bloomington Stock center or Tsinghua Fly center, and a full list of genotypes is provided as Appendix Table S3.

### Ovarian cell suspension for scRNA-seq

Newly emerged virgin female flies were fed for 1 week to encourage ovarian growth, then 150 flies were dissected in a petri dish containing 1 ml of S-FBS (Serum-free Schneider's insect medium (Sigma-Aldrich, cat. no. S0146) supplemented with 10% (v/v) fetal bovine serum (FBS), heat inactivated (Sigma-Aldrich, cat. no. F4135) under the microscope (Leica, SAPO, Germany)). After dissection, S-FBS was discarded, and 1 ml of PBS was added to rinse ovaries in a 1.5-ml centrifuge tube. Samples were allowed to settle for 5 min and then rinsed twice with PBS. Dissociation was carried out at room temperature in 700  $\mu$ l of dissociation medium by adding 70  $\mu$ l of 5% (w/v) trypsin (Invitrogen, cat. no. 27250-018) and 70  $\mu$ l of 2.5% (w/v) collagenase (Invitrogen, cat. no. 17018029) to 560  $\mu$ l of PBS, and incubated for 15 min with continuous shaking. After incubation, the ovarian cell suspension was pipetted into a 40- $\mu$ m mesh cell strainer, and filtered suspension into a 1.5-ml centrifuge tube containing 500  $\mu$ l of S-FBS. Then, the empty tube and cell strainer were washed by 100  $\mu$ l of S-FBS respectively to collect the remaining cells. The cell suspension was collected by centrifuging for 5 min at 425  $\times$  g, 4°C. Then the S-FBS was discarded, and the pellets were resuspended with 200  $\mu$ l of serum-free Schneider's insect medium, and the suspensions were combined into one tube. Next, the cell viability was examined by using 0.4% trypan blue (Solarbio, cat. no. T8070) at a proportion of 1:1, and counted by a

hemocytometer. The concentration of cell suspension was  $1.37 \times 10^6$  cells/ml, and the viability was 90% at least, in line with the recommendations from 10× Genomics.

### Single-cell RNA sequencing

Single-cell libraries were constructed using chromium single-cell 3' Library (v2) kit via End Repair, A-tailing, Adaptor Ligation, and PCR according to the manufacturer's protocol. In brief, the cells of each group were mixed into one sample and adjusted to 1,000 cell/ $\mu$ l. Then, the indexed sequencing libraries which contained the P5 and P7 primers were prepared using chromium single-cell 3' Reagent kit, and the barcoded sequencing libraries were quantified using a standard curve-based qPCR assay (KAPA Biosystems, USA) and Agilent Bioanalyzer 2100 (Agilent, Loveland, CO, USA). Subsequently, the library sequencing was performed by Illumina HiSeq 4000 with a custom paired-end sequencing mode 26 bp (read 1)  $\times$  98 bp (read 2).

### 10× genomics initial quality control

The scRNA-seq data were processed with the Cell Ranger Single Cell Software Suite (v6.1; <http://software.10xgenomics.com/single-cell/overview/welcome>) for quality control, sample demultiplexing, barcode processing, and single-cell 3' gene counting. First, the raw data were demultiplexed by using an 8 bp index read at the end of Read 1 and Read 2 paired-end reads, to generate FASTQ files, and then quality control was performed using FastQC, and these data were aligned against the Nucleotide Sequence Database (<https://www.ncbi.nlm.nih.gov/genbank/>) using the NCBI Basic Local Alignment Search Tool (BLAST). Second, the reads were aligned to the *Drosophila* reference genome (dm6; [https://www.ncbi.nlm.nih.gov/assembly/GCF\\_000001215.4#/st](https://www.ncbi.nlm.nih.gov/assembly/GCF_000001215.4#/st)) by STAR RNA-Seq aligner. Once aligned, barcodes associated with these reads-UMIs were subjected to filtering and correction. For UMI tag counting, the 10× Genomics pipeline Cell Ranger was used to generate single-cell gene counts for each library. The confidently mapped, non-PCR duplicates with valid barcodes and UMIs were eventually used to generate the gene-barcode matrix. For the higher depth libraries, the samples were normalized to the sample sequencing depth. Cell Ranger version 2.0.0 and Seurat (v4.0.4; Hao et al, 2021) R packages were used to filter out the low-quality cells, and the following criteria were used to filter cells: (i) gene counts > 3000 per cell; (ii) UMI counts > 12,000 per cell; and (iii) percentage of mitochondrial genes > 30%. In this study, the estimated cell number was derived by plotting the UMI counts against the barcodes and revealed 21,755 cells used for downstream analysis. Based on the transcriptomes of 21,755 cells, a total of 0.39 billion clean reads achieving an average read of 18,202 per cell and the ratio of high-quality reads to qualify scores at Q30 was more than 90.6% were obtained. The total number of read pairs that were assigned to this library in demultiplexing is 395,988,785, and the valid Barcodes (fraction of reads with barcodes that match the whitelist after barcode correction) and valid UMIs (unique molecular identifier) are 97.8 and 100%, respectively. The number of estimated cells is 21,755 with 18,202 mean reads per cell, and the number of median genes per cell was 638. The rough sequencing data were filtered according to the criterion that any cell containing more than 25,000 UMIs counts and more

than 30% mitochondrial UMIs was filtered out. We finally obtained 8,497 out of 21,755 cells with 3,993 median UMIs per cell and 868 median genes per cell (Appendix Table S1) for scRNA-seq analysis.

### Cluster analysis

For the clustering, we used principal component analysis (PCA) to normalize and filter the gene-barcode matrix and to reduce feature dimensions. The top five major components were selected to obtain the visualized 2D clustering image using T-distributed stochastic neighbor embedding (tSNE). The graph-based clustering method was applied to group cells with similar expression patterns of marker genes. The ovarian cell clusters were grouped into 24 unsupervised categories using the different resolution parameters ( $R = 0.5$  or default values). The pairwise Pearson correlation was calculated between each cluster for hierarchical clustering. Based on the differentially expressed gene results, a visualized heat map was created using the Seurat (v4.0.4) R package. The tSNE plot was generated for a graphical representation of specific gene expression by Loupe Cell Browser software and Seurat (v4.0.4) R package. Notably, in order to improve the accuracy of trajectory based on our clustering results, we removed the cells which expressed somatic cell marker *tj*, and non-*vasa* (*vas*) expressing cells in germline clusters.

### Marker gene analysis and monocle pseudotime analysis

The candidate marker genes which enriched in a specific cluster were selected according to the expression profile of top genes among 24 clusters, and the putative biological identity of each cluster was assigned based on the expression patterns of highly expressed genes and experimentally validated markers. Single-cell pseudotime analysis was carried out by using matrices of cells and gene expression by Monocle (v2.20.0) which provided the visualized trajectory with tips and branches in the reduced dimensional space.

### Differential gene expression analysis

The likelihood-ratio test (Laurens & Hinton, 2008) was used to seek differential expression profiles in each cluster, and the following criterion were allowed to identify the differentially expressed genes: (i)  $P$ -value  $\leq 0.01$ . (ii)  $\text{Log}_2(\text{fold change [FC]}) \geq 0.360674$ . (iii) The percentage of cells where the gene is detected in a specific cluster > 25%. Then, Gene Ontology (GO) enrichment analysis was performed to filter the differentially expressed genes that correspond to biological functions. The peak-related genes were mapped to GO terms in the GO database (<http://www.geneontology.org/>), and the significantly enriched GO terms were defined by a hypergeometric test. To further understand the biological functions of these genes, we used Kyoto Encyclopedia of Genes and Genomes (KEGG; <https://www.kegg.jp/>) pathway enrichment analysis to identify the enriched metabolic pathways and signal transduction pathways.

### RNAi screen

For the genetic RNAi experiments, we used  $y^1w^{118}$ , *nos-Gal4/CyO*; *tub-Gal80<sup>ts</sup>/TB* to cross with *UAS-RNAi* lines, and maintained the

flies at 18°C. Then the eggs were continually collected and kept at 18°C. After eclosion, the adult flies were transferred to 29°C to fully drive the expression of *UAS-RNAi* transgenes and fed for 7 days.

### Gene regulatory network analysis

The transcription factor network inference was conducted by the SCENIC R package. The log-normalized expression was generated by using Seurat, and the pipeline was implanted step by step. Preliminarily, the gene coexpression was identified via GENIE3, which may include some false positives and indirect targets. Then, putative direct-binding targets were identified by pruning each coexpression module via Rcis Target. Networks (regulons) were retained if the TF-binding motif was enriched among its targets, while target genes without direct TF-binding motifs were removed. Last, the activity of each regulon was scored for each single cell via the AUC scores using AUCCell R package.

The *Cytoscape* v.3.9.1 software was applied for the construction of gene regulatory network according to its online user manual.

### RNA *in situ* hybridization

The probes were synthesized using the genomic DNA as a template and amplifying the exon regions of targeted genes by using the primers with SP6 sequence (ATTTAGGTGACACTATAGAAGNG) according to the product description of KAPA HiFi PCR Kit (Roche Diagnostics, cat. no. 07958927001). Sense and antisense digoxigenin (DIG)-labeled probes were synthesized from the purified PCR product using DIG RNA Labeling Kit (Roche, cat. no.11175025910). All primer sequences are listed in Appendix Table S6.

The procedures for RNA *in situ* hybridization were as follows. Briefly, the samples were dissected in PBS and immediately fixed in 4% PFA with 0.1 M Hepes at 4°C overnight. On the next day, the samples were washed 3 × 10 min with PBST (0.1% Tween 20 in PBS) and dehydrated with sequential washes with 50 and 100% methanol in PBST for 5 min each time. Then, the samples were stored in the −20°C refrigerator for 40 min and washed with PBST 3 × 10 min before proteinase K (Sigma-Aldrich, cat. no. 39450016) treatment for 5 min at room temperature. Samples were washed with PBS for 5 min and fixed with 4% PFA for 20 min, then washed with PBST 3 × 10 min and incubated in hybridization buffer (50% formamide, 5× SSC, 0.1% Tween-20, 50 µg/µl heparin, and 100 µg/ml salmon sperm DNA) with probe in hybridization oven (Jingxin Industrial Development Co. Ltd, LF-1) at 60°C for 24 h at least. After hybridization, the samples were washed 4 × 30 min at 60°C, once with 2× SSCT (2× SSC, 0.1% Tween-20) for 15 min and twice with 0.2× SSCT (0.2× SSC, 0.1% Tween-20) for 30 min each at 60°C. Next, samples were washed with MABT (0.1 M maleic acid; 0.15 M NaCl PH 7.4 and 0.1% Tween-20) 2 × 10 min at room temperature and blocked for at least 30 min, and then added anti-dig-POD (1:200; Roche, cat. no.11207733910) in 5% blocking solution (Roche, cat. no.11096176001) at room temperature overnight. Finally, the fluorescence reaction was carried out by using TSA fluorescein system (Perkin Elmer, cat. no. TS-000100) for 1.5 h in dark and subsequently used Hoechst 33258 (Sigma-Aldrich, cat. no. 23491454) to label the nucleus.

### Construction of transgenic fly lines

We first designed guide RNA targets with: (i) Chopchop (<https://chopchop.cbu.uib.no/>; Labun *et al*, 2019), (ii) CCTop (<https://cctop.cos.uni-heidelberg.de/>; Labuhn *et al*, 2018). Genomic DNA was isolated from the injection stock. PCR was performed using primers flanking the targets. The amplified products were sent for Sanger sequencing. If SNPs were found on the targets, gRNA sequence would be modified to be consistent with the target sequence of the stock.

The first base of gRNA sequence was changed to G for the T7 transcription. Following the protocol (Bassett *et al*, 2014), the template for *in vitro* transcription by T7 polymerase was generated by annealing of two DNA oligonucleotides and PCR amplification. *In vitro* transcription was performed with the T7 RiboMAX™ Kit (Promega, cat. no. P1320). Transcripts were purified by phenol-chloroform extraction and isopropanol precipitation.

Plasmid MLM3613 (Addgene plasmid, cat. no. 42251) was linearized with *Pme* I (New England Biolabs) and purified by ethanol precipitation. Cas9 mRNA was transcribed with mMACHINE® T7 Transcription Kit (Ambion, cat. no. C013843), polyadenylated with the *Escherichia coli* Poly (A) polymerase Kit (NEB, cat. no. M0276L), and purified with the RNeasy Mini Kit (QIAGEN, cat. no. 74106).

To knock in the 6 × HA of GFP in the N-terminal of *eggpl*, the pBluescript SK vector (pBS) was used as the backbone. Using genomic DNA of the injection stock, the homology 5' arm and 3' arm was amplified and linked to the pBS backbone with Gibson Assembly Kit (NEB, cat. no.E2611L) as “pBS-CG32814-arm.” Then the pBS-*eggpl*-arm was linearized by PCR and linked to the GFP-6HA cassette with Gibson Assembly Kit (Thermo Fisher, cat. no. A46624), and that produced the final donor construct “pBS-CG32814-GFP-6HA” (Fig EV3A).

To generate a mutant allele of *eggpl*, we used Cas9/CRISPR to introduce mutations downstream of the ATG in the *eggpl* open reading frame. We identified an allele, *eggpl*<sup>l11</sup> in which the 5 base pairs immediately downstream from the ATG (AGTAG) were deleted and a 28-base pair region that is 50 base pairs downstream from the ATG (TTAAAACGGACACCATCGGCGAAGAAAA) contained multiple deletions and substitutions. In *eggpl*<sup>l11</sup>, this 28 base pair region was instead an 18 base pair region with the following sequence: CTTCTTACCATTTCAC. The resulting allele contains several frameshifts that alter the coding sequence of the 5' end of the gene but restore the normal reading frame after the 27<sup>th</sup> codon. The DNA sequence of this mutated region in the *eggpl*<sup>l11</sup> allele, starting at the ATG of the open reading frame, is ATG-----CGGAATCATTTTCAGACAGAAATCCAGATGGATCTTTTTCACCTTCTt---C-ttACCATTttC-----AcC. Dashes indicate the location of deletions and lowercase letters indicate substitutions, relative to the wildtype sequence. The gRNA sequences are list below:

CG32814-sg1: GTTAGAATCAAAATGAGTAG

CG32814-sg2: GCTTTTAAAACGGACACCAT

The primers for validation were GGAGTCTCCAGCAATTACTGTAT and CCCTGATTGCAATGAGTTTTCAGT.

Fifteen micrograms of Cas9 mRNA and 7.5 µg sgRNA were mixed with DEPC water in a 30 µl volume. And the RNA mix injection was performed by Qidong Fungene Biotechnology (<http://www.fungene.tech>). 300 embryos were injected.



When the injected P0 embryos grew into adults, they were crossed with Fm7a. The genomic DNA of the P0 and F1 flies was extracted. PCR was performed using primers for validation of mRuby3 insertion:

F: AAGTTGTCAGCCGATTGGCGTGG

R: ATTCACTTTTCATTATTGAATG

The F2 flies from positive F1 tubes were balanced with *Fm7a*.

Transgenic fly lines w\*; P{UAS-*eggpl*-GFP}attP2/TM6B was generated by integrating *UAS-eggpl-GFP* into the attP2 site. Briefly, the NotI/XbaI PCR fragment of *eggpl*-CDS (GFP tag) was cloned into the NotI/XbaI sites of pJFRC28-10 × UAS-IVS-GFP-p10 vector (Addgene Plasmid, cat. no. 36431). The primer pairs used for PCR validation were as following:

*eggpl*-3F: ACAACAAGCCATATGATGAG

p10-R: GCCACTAGCTCGCTATACACT

### Whole-mount immunofluorescence staining and confocal imaging

Ovaries were dissected in PBS and fixed in 4% PFA, 0.1 M Hepes, PH 7.4 for 30 min at room temperature with gentle rotation, then washed the ovaries 3 × 15 min with 500 μl 0.1% PBT (0.1% Triton X-100 in PBS). The samples were blocked in 5% NGS buffer (5% normal goat serum in 0.1% PBT) for 1 h before incubation with primary antibody at room temperature overnight. The following day, diluted primary antibody was collected for reuse, and the samples were washed 3 × 15 min with 500 μl PBT and incubated with diluted secondary antibody for 3 h with rotation. The Hoechst labeling was performed after washing with PBT 3 × 15 min. Finally, the samples were mounted on slides in Vectashield mounting medium and stored at 4°C. Note that, 50% normal goat serum in 0.1% PBT and higher concentration of diluted primary antibody were recommended to apply for the continuous antibody staining procedure after RNA *in situ* hybridization. For pMad staining, the samples were suggested to fix in 4% PFA for 50 min and washed the ovaries with 0.1% PBT three times for 3 h at least.

The following primary antibodies were applied in this study: mouse anti- $\alpha$ -Spectrin (3A9, 1:100; Developmental Studies Hybridoma Band (DSHB)), rabbit anti-pMad (1:800; Cell Signaling), chicken anti-GFP (1:5,000; Abcam), rat anti-Vasa (1:100, DSHB), rabbit anti-PH3 (1:200, Cell Signaling Technology), and rabbit anti-Caspase 3 (1:2,000, Cell Signaling). Alexa Fluor 488, 555, or 633 conjugated goat secondary antibodies (gifts from Yu. Cai, Temasek Life Sciences Laboratory, Singapore) against mouse (1:500), rabbit (1:1,000), chicken (1:500) and rat (1:1,000) were used to detect the primary antibodies. Polyclonal anti-TfIIA-S and anti-*eggpl* were generated via immunization of rabbits (Custom made for chickens by GeneCreate Biotech Co., Wuhan, China, 1:1,000). The DNA dyes Hoechst 33258 (1:5,000; Cell Signaling Technology) was used to label the nucleus.

To perform TUNEL assay, the ovaries were fixed in 4% PFA for 1 h and rinsed three times with PBS for 30 min. Then, the samples were incubated in permeabilization solution for 2 min on ice. To prepare 50 μl TUNEL reaction mixture with 5 μl of enzyme solution and 45 μl label solution and incubated the samples for 1 h at 37°C and then, carrying on the standard immunostaining procedures as described.

Images were captured by using the Nikon A1 plus confocal microscope (Nikon, Japan) with APO 60×/1.40 oil objective lens at

room temperature, and all images were processed with NIS-Elements software for image acquisition and analysis. The mean of fluorescence intensity was examined by using ImageJ v1.8.0 software according to the manual instruction (Fig EV3C) or Imaris (Fig 5L and M). For image analysis in Imaris, surfaces were generated in the green (GFP) channel and manually split or merged to generate a single surface for each cyst in Region 1. Then, the mean pixel intensity in the green channel within each surface was calculated.

### BrdU incorporation

5-Bromo-2'-deoxyuridine (BrdU), an analog of the nucleoside thymidine, was used in examining the frequency of the S-phase during cellular cycle in this study. The BrdU (Sigma-Aldrich, cat. no. B5002) saturated solution was freshly diluted with 200 μl PBS (10 mM) and 800 μl dehydrated alcohol. The female flies were dissected in petri dish containing 1 mL Schneider's insect medium at room temperature, then the ovaries were carefully transferred into a 12-well plate with the mixture of BrdU solution and Schneider's insect medium (1:100) for further incubation at 25°C. After 45 min, the ovaries were rinsed with Schneider's insect medium two times, washed with PBS for 5 min, and fixed in 4% PFA for 50 min. The samples were washed 2 × 10 min with 0.3% PBT (0.3% Triton X-100 in PBS), and then washed with 0.6% PBT (0.6% Triton X-100 in PBS) for 45 min. Next, ovaries were acid treated with 1 ml 0.6% PBT and 1 ml 3.2 mol/l HCL for 30 min and then the washed with 0.3% PBT 3 × 10 min and 0.1% PBT for 30 min. The ovaries were blocked with 10% NGS (10% normal goat serum in 0.1% PBT) for 1 h and incubated with 1:50 mouse anti-BrdU monoclonal antibody (Becton Dickinson cat. no. 7580) at 4°C, overnight. The next step was followed by the standard immunofluorescence staining procedure described above.

### Protein overexpression of *eggpl* in Sf9 cell line *in vitro*

The Sf9 cell line was a gift from the State Key Laboratory for Biocontrol and Institute of Entomology, Sun Yat-sen University, China. Briefly, the ORF of *eggpl* was inserted into vector piztv5-His (Novagen) in our laboratory to overexpress *eggpl*, and cell co-transfection was carried out using FuGENE HD Transfection Reagent (Promega). Then, Sf9 cell line was maintained at 28°C in 25 cm<sup>2</sup> culture flasks (Nest, China) in Grace's insect cell culture medium containing 10% fetal bovine serum (Gibco, USA).

### Egg-laying assay

The newly emerged 10 male adult flies and 10 female flies were fed in 28.5 × 95 mm vials (cat: 51-0800, Biologix) containing with the standard food and kept in the incubator at 25°C. The flies were provided with fresh food every day for 21 days. The vials from the previous day, which contained the laid eggs, were collected, and the number of laid eggs was counted under the stereomicroscope (Leica, S APO). Three biological replicates were performed in this assay.

### Statistical analysis

All data were analyzed by one-way ANOVA with *Duncan's* multiple range test (DMRT) using a SAS statistical windows 8.1 package

program (Microsoft, USA).  $P < 0.05$  was considered to be statistically significant. Image J V1.8.0 software was used to measure the ovary size.

## Data availability

The datasets produced in this study are available in Gene Expression Omnibus (GEO, NCBI) with databases accession number GSE210822 (<https://www.ncbi.nlm.nih.gov/geo/query/acc.cgi?acc=GSE210822>).

**Expanded View** for this article is available [online](#).

## Acknowledgements

This work was supported by National Natural Science Foundation of China (No. 31572335). TGN was supported by the National Institute of General Medical Sciences of the National Institutes of Health under Award Number R35GM136348. The content is solely the responsibility of the authors and does not necessarily represent the official views of the National Institutes of Health. We gratefully thank Guangzhou Genedenovo Biotechnology Co., Ltd for the assistance in sequencing and bioinformatics analysis. Specially thank for the generous help and professional guidance provided by Suning Liu (South China Normal University, China).

## Author contributions

**Zhipeng Sun:** Conceptualization; formal analysis; validation; investigation; visualization; methodology; writing – original draft; writing – review and editing. **Todd G Nystul:** Formal analysis; supervision; funding acquisition; investigation; writing – original draft; project administration; writing – review and editing. **Guohua Zhong:** Conceptualization; supervision; funding acquisition; writing – original draft; project administration; writing – review and editing.

## Disclosure and competing interests statement

The authors declare that they have no conflict of interest.

## References

- Alic N, Andrews TD, Giannakou ME, Papatheodorou I, Slack C, Hoddinott MP, Cochemé HM, Schuster EF, Thornton JM, Partridge L (2011) Genome-wide dFOXO targets and topology of the transcriptomic response to stress and insulin signalling. *Mol Syst Biol* 7: 502
- Ameku T, Niwa R (2016) Mating-induced increase in germline stem cells via the neuroendocrine system in female *Drosophila*. *PLoS Genet* 12: e1006123
- Andersen PR, Tirian L, Vunjak M, Brennecke J (2017) A heterochromatin-dependent transcription machinery drives piRNA expression. *Nature* 549: 54–59
- Banisch TU, Maimon I, Dadosh T, Gilboa L (2017) Escort cells generate a dynamic compartment for germline stem cell differentiation via combined Stat and Erk signalling. *Development* 144: 1937–1947
- Bassett A, Tibbit C, Ponting C, Liu JL (2014) Highly efficient targeted mutagenesis of *Drosophila* with the CRISPR/Cas9 system. *Cell Rep* 6: 1178–1179
- Blatt P, Martin ET, Breznak SM, Rangan P (2020) Post-transcriptional gene regulation regulates germline stem cell to oocyte transition during *Drosophila* oogenesis. *Curr Top Dev Biol* 140: 3–34
- Buszczak M, Paterno S, Spradling AC (2009) *Drosophila* stem cells share a common requirement for the histone H2B ubiquitin protease scrawny. *Science* 323: 248–251
- Casale AM, Cappucci U, Piacentini L (2021) Unravelling HP1 functions: post-transcriptional regulation of stem cell fate. *Chromosoma* 130: 103–111
- Clough E, Tedeschi T, Hazelrigg T (2014) Epigenetic regulation of oogenesis and germ stem cell maintenance by the *Drosophila* histone methyltransferase Eggless/dSetDB1. *Dev Biol* 388: 181–191
- Dansereau DA, Lasko P (2008) The development of germline stem cells in *Drosophila*. In *Methods in Molecular Biology*, Hou SX, Singh SR (eds), pp 3–26. Totowa, NJ: Humana Press
- Deshpande G, Calhoun G, Yanowitz JL, Schedl PD (1999) Novel functions of nanos in downregulating mitosis and transcription during the development of the *Drosophila* germline. *Cell* 99: 271–281
- Drummond-Barbosa D (2019) Local and physiological control of germline stem cell lineages in *Drosophila melanogaster*. *Genetics* 213: 9–26
- Drummond-Barbosa D, Spradling AC (2001) Stem cells and their progeny respond to nutritional changes during *Drosophila* oogenesis. *Dev Biol* 231: 265–278
- Eichler CE, Hakes AC, Hull B, Gavis ER (2020) Compartmentalized oskar degradation in the germ plasm safeguards germline development. *Elife* 9: e49988
- Flores HA, Dumont V, Fadoo A, Hubbard D, Aquadro CF (2015) Adaptive evolution of genes involved in the regulation of germline stem cells in *Drosophila melanogaster* and *D. simulans*. *G3 (Bethesda)* 5: 583–592
- Fu Z, Geng C, Wang H, Yang Z, Weng C, Li H, Deng L, Liu L, Liu N, Ni J et al (2015) Twin promotes the maintenance and differentiation of germline stem cell lineage through modulation of multiple pathways. *Cell Rep* 13: 1366–1379
- Hao Y, Hao S, Andersen-Nissen E, Mauck WM, Zheng S, Butler A, Lee MJ, Wilk AJ, Darby C, Zager M et al (2021) Integrated analysis of multimodal single-cell data. *Cell* 184: 3573–3587
- Hinnant TD, Alvarez AA, Ables ET (2017) Temporal remodeling of the cell cycle accompanies differentiation in the *Drosophila* germline. *Dev Biol* 429: 118–131
- Hinnant TD, Merkle JA, Ables ET (2020) Coordinating proliferation, polarity, and cell fate in the *Drosophila* female germline. *Front Cell Dev Biol* 8: 19
- Hsu HJ, Drummond-Barbosa D (2009) Insulin levels control female germline stem cell maintenance via the niche in *Drosophila*. *Proc Natl Acad Sci USA* 106: 1117–1121
- Hsu HJ, Lafever L, Drummond-Barbosa D (2008) Diet controls normal and tumorous germline stem cells via insulin-dependent and -independent mechanisms in *Drosophila*. *Dev Biol* 313: 700–712
- Jevitt A, Chatterjee D, Xie G, Wang XF, Otwell T, Huang YC, Deng WM (2020a) A single-cell atlas of adult *Drosophila* ovary identifies transcriptional programs and somatic cell lineage regulating oogenesis. *PLoS Biol* 18: e3000538
- Jevitt A, Chatterjee D, Xie G, Wang XF, Otwell T, Huang YC, Deng WM (2020b) Gene Expression Omnibus GSE146040. (<https://www.ncbi.nlm.nih.gov/geo/query/acc.cgi?acc=GSE146040>). [DATASET]
- Ji Y, Tulin AV (2012) Poly(ADP-ribose) controls DE-cadherin-dependent stem cell maintenance and oocyte localization. *Nat Commun* 3: 760
- Kahney EW, Snedeker JC, Chen X (2019) Regulation of *Drosophila* germline stem cells. *Curr Opin Cell Biol* 60: 27–35
- Kim-Ha J, Smith JL, Macdonald PM (1991) oskar mRNA is localized to the posterior pole of the *Drosophila* oocyte. *Cell* 66: 23–35
- König A, Yatsenko AS, Weiss M, Shcherbata HR (2011) Ecdysteroids affect *Drosophila* ovarian stem cell niche formation and early germline differentiation. *EMBO J* 30: 1549–1562

- Labuhn M, Adams FF, Ng M, Knoess S, Schambach A, Charpentier EM, Schwarzer A, Mateo JL, Klusmann JH, Heckl D et al (2018) Refined sgRNA efficacy prediction improves large- and small-scale CRISPR-Cas9 applications. *Nucleic Acids Res* 46: 1375–1385
- Labun K, Montague TG, Krause M, Torres Cleuren YN, Tjeldnes H, Valen E (2019) CHOPCHOP v3: expanding the CRISPR web toolbox beyond genome editing. *Nucleic Acids Res* 47: 171–174
- LaFever L, Drummond-Barbosa D (2005) Direct control of germline stem cell division and cyst growth by neural insulin in *Drosophila*. *Science* 309: 1071–1073
- Lasko PF, Ashburner M (1988) The product of the *Drosophila* gene vasa is very similar to eukaryotic initiation factor-4A. *Nature* 335: 611–617
- Laurens VD, Hinton G (2008) Visualizing data using t-SNE. *J Mach Learn Res* 9: 2579–2605
- Li Y, Zhang Q, Carreira-Rosario A, Maines JZ, McKearin DM, Buszczak M (2013) Mei-P26 Cooperates with Bam, Bgcn and Sxl to promote early germline development in the *Drosophila* ovary. *PLoS ONE* 8: e58301
- Li H, Janssens J, De Waegeneer M, Kolluru SS, Davie K, Gardeux V, Saelens W, David FPA, Brbić M, Spanier K et al (2022) Fly Cell Atlas: a single-nucleus transcriptomic atlas of the adult fruit fly. *Science* 375: eabk2432
- Liu M, Lim TM, Cai Y (2010) The *Drosophila* female germline stem cell lineage acts to spatially restrict DPP function within the niche. *Sci Signal* 3: ra57
- Lu T, Wang S, Gao Y, Mao Y, Yang Z, Liu L, Song X, Ni J, Xie T (2015) COP9-Hedgehog axis regulates the function of the germline stem cell progeny differentiation niche in the *Drosophila* ovary. *Development* 142: 4242–4252
- Maines JZ, Park JK, Williams M, McKearin DM (2007) Stonewalling *Drosophila* stem cell differentiation by epigenetic controls. *Development* 134: 1471–1479
- Ohlstein B, Lavoie CA, Vef O, Gateff E, McKearin DM (2000) The *Drosophila* cystoblast differentiation factor, benign gonial cell neoplasm, is related to DExH-box proteins and interacts genetically with bag-of-marbles. *Genetics* 155: 1809–1819
- Page SL, Khetani RS, Lake CM, Nielsen RJ, Jeffress JK, Warren WD, Bickel SE, Hawley RS (2008) Corona is required for higher-order assembly of transverse filaments into full-length synaptonemal complex in *Drosophila* oocytes. *PLoS Genet* 4: e1000194
- Panchal T, Chen X, Alchits E, Oh Y, Poon J, Kouptsova J, Laski FA, Godt D (2017) Specification and spatial arrangement of cells in the germline stem cell niche of the *Drosophila* ovary depend on the Maf transcription factor *Traffic jam*. *PLoS Genet* 13: e1006790
- Perinhotathil S, Kim C (2011) Bam and Bgcn in *Drosophila* germline stem cell differentiation. *Vitam Horm* 87: 399–416
- Rastegari E, Kajal K, Tan BS, Huang F, Chen RH, Hsieh TS, Hsu HJ (2020) WD40 protein Wuho controls germline homeostasis via TRIM-NHL tumor suppressor Mei-p26 in *Drosophila*. *Development* 147: dev182063
- Rhiner C, Díaz B, Portela M, Poyatos JF, Fernández-Ruiz I, López-Gay JM, Gerlitz O, Moreno E (2009) Persistent competition among stem cells and their daughters in the *Drosophila* ovary germline niche. *Development* 136: 995–1006
- Rust K, Byrnes LE, Yu KS, Park JS, Sneddon JB, Tward AD, Nystul TG (2020a) A single-cell atlas and lineage analysis of the adult *Drosophila* ovary. *Nat Commun* 11: 5628
- Rust K, Byrnes LE, Yu KS, Park JS, Sneddon JB, Tward AD, Nystul TG (2020b) Gene Expression Omnibus GSE136162. (<https://www.ncbi.nlm.nih.gov/geo/query/acc.cgi?acc=GSE136162>). [DATASET]
- Satija R, Farrell JA, Gennert D, Schier AF, Regev A (2015) Spatial reconstruction of single-cell gene expression data. *Nat Biotechnol* 33: 495–502
- Scholz H, Franz M, Heberlein U (2005) The *hangover* gene defines a stress pathway required for ethanol tolerance development. *Nature* 436: 845–847
- Schulz C, Wood CG, Jones DL, Tazuke SI, Fuller MT (2002) Signaling from germ cells mediated by the rhomboid homolog *stet* organizes encapsulation by somatic support cells. *Development* 129: 4523–4534
- Shi J, Jin Z, Yu Y, Zhang Y, Yang F, Huang H, Cai T, Xi R (2021) A progressive somatic cell niche regulates germline cyst differentiation in the *Drosophila* ovary. *Curr Biol* 31: 840–852
- Silver DL, Montell DJ (2001) Paracrine signaling through the JAK/STAT pathway activates invasive behavior of ovarian epithelial cells in *Drosophila*. *Cell* 107: 831–841
- Singh PK, Hollingsworth MA (2006) Cell surface-associated mucins in signal transduction. *Trends Cell Biol* 16: 467–476
- Slaidina M, Gupta S, Banisch TU, Lehmann R (2021) A single-cell atlas reveals unanticipated cell type complexity in *Drosophila* ovaries. *Genome Res* 31: 1938–1951
- Slaidina M, Lehmann R (2021) Gene Expression Omnibus GSE162192. (<https://www.ncbi.nlm.nih.gov/geo/query/acc.cgi?acc=GSE162192>). [DATASET]
- Steinhauer WR, Kalfayan LJ (1992) A specific ovarian tumor protein isoform is required for efficient differentiation of germ cells in *Drosophila* oogenesis. *Genes Dev* 6: 233–243
- Su YH, Rastegri E, Kao SH, Lai CM, Hsu HJ (2018) Diet regulates membrane extension and survival of niche escort cells for germline homeostasis via insulin signaling. *Development* 145: dev159186
- Sun J, Deng WM (2005) Notch-dependent downregulation of the homeodomain gene *cut* is required for the mitotic cycle/endocycle switch and cell differentiation in *Drosophila* follicle cells. *Development* 132: 4299–4308
- Sun J, Wei HM, Xu J, Chang JF, Yang Z, Ren X, Lv WW, Liu LP, Pan LX, Wang X et al (2015) Histone H1-mediated epigenetic regulation controls germline stem cell self-renewal by modulating H4K16 acetylation. *Nat Commun* 6: 8856
- Tarikere S, Ylla G, Extavour CG (2022) Distinct gene expression dynamics in germ line and somatic tissue during ovariole morphogenesis in *Drosophila melanogaster*. *G3 (Bethesda)* 12: jkab305
- Tatapudy S, Peralta J, Nystul T (2021) Distinct roles of Bendless in regulating FSC niche competition and daughter cell differentiation. *Development* 148: dev199630
- Tazuke SI, Schulz C, Gilboa L, Fogarty M, Mahowald AP, Guichet A, Ephrussi A, Wood CG, Lehmann R, Fuller MT (2002) A germline-specific gap junction protein required for survival of differentiating early germ cells. *Development* 129: 2529–2539
- Tu R, Duan B, Song X, Chen S, Scott A, Hall K, Blanck J, DeGraffenreid D, Li H, Perera A et al (2021) Multiple niche compartments orchestrate stepwise germline stem cell progeny differentiation. *Curr Biol* 31: 827–839
- Tzolovsky G, Deng WM, Schlitt T, Bownes M (1999) The function of the broad-complex during *Drosophila melanogaster* oogenesis. *Genetics* 153: 1371–1383
- Upadhyay M, Kuna M, Tudor S, Martino Cortez Y, Rangan P (2018) A switch in the mode of Wnt signaling orchestrates the formation of germline stem cell differentiation niche in *Drosophila*. *PLoS Genet* 14: e1007154
- Urwyler O, Cortinas-Elizondo F, Suter B (2012) *Drosophila* sosie functions with  $\beta$ (H)-Spectrin and Actin organizers in cell migration, epithelial morphogenesis and cortical stability. *Biol Open* 1: 994–1005

- Vidaurre V, Chen X (2021) Epigenetic regulation of *Drosophila* germline stem cell maintenance and differentiation. *Dev Biol* 473: 105–118
- Wang L, Cai LY (2008) The JAK/STAT pathway positively regulates DPP signaling in the *Drosophila* germline stem cell niche. *J Cell Biol* 180: 721–728
- Wang X, Pan L, Wang S, Zhou J, McDowell W, Park J, Haug J, Staehling K, Tang H, Xie T (2011) Histone H3K9 trimethylase Eggless controls germline stem cell maintenance and differentiation. *PLoS Genet* 7: e1002426
- Witt E, Benjamin S, Svetec N, Zhao L (2019) Testis single-cell RNA-seq reveals the dynamics of *de novo* gene transcription and germline mutational bias in *Drosophila*. *Elife* 8: e47138
- Xie T (2013) Control of germline stem cell self-renewal and differentiation in the *Drosophila* ovary: concerted actions of niche signals and intrinsic factors. *Wiley Interdiscip Rev Dev Biol* 2: 261–273
- Xie T, Spradling AC (1998) decapentaplegic is essential for the maintenance and division of germline stem cells in the *Drosophila* ovary. *Cell* 94: 251–260
- Xie T, Spradling A (2001) The *Drosophila* ovary: an in vivo stem cell system. In *Stem Cell Biology*, Marshak DR, Gardner RL, Gottlieb D (eds), pp 129–148. Cold Spring Harbor, NY: Cold Spring Harbor Laboratory Press
- Yoshinari Y, Ameku T, Shu K, Tanimoto H, Niwa R (2020) Neuronal octopamine signaling regulates mating-induced germline stem cell increase in female *Drosophila melanogaster*. *Elife* 9: e57101